

A New Method of Modelling Tunable Lasers with Functional Composition

by

Brady Metherall

A Thesis Submitted in Partial Fulfillment
of the Requirements for the Degree of
Master of Science
in
The Faculty of Science
Modelling and Computational Science

University of Ontario Institute of Technology

July 2019



© Brady Metherall 2019

Abstract

A new nonlinear model is proposed for tuneable lasers. Using the generalized nonlinear Schrödinger equation as a starting point, expressions for the transformations undergone by the pulse are derived for each of the five components (gain, loss, dispersion, modulation, and nonlinearity) within the laser cavity. These transformations are then composed to give the overall effect of one trip around the cavity. We first examine the linearized version of the model which is solved analytically. Then the full nonlinear model is solved numerically. A consequence of the nonlinear nature of this model is that it is able to exhibit wave breaking which prior models could not. We highlight the rich structure of the boundary of stability for a particular plane of the parameter space.

Acknowledgements

First and most importantly, I would like to thank my supervisor and mentor, Dr. Sean Bohun, for his assistance, guidance, and inspiration over the past two years. I would also like to thank my fellow modelling and computational science students for helping make the last two years enjoyable.

Lastly, I would like to thank my mom and dad, and grandparents for their endless support and encouragement over the past two years.

Author's Declaration

I declare that the work in this thesis was carried out in accordance with the regulations of the University of Ontario Institute of Technology. The work is original except where indicated by special reference in the text and no part of the dissertation has been submitted for any other degree. Any views expressed in the dissertation are those of the author and in no way represent those of the University of Ontario Institute of Technology. This thesis has not been presented to any other university for examination either in Canada or elsewhere.

Brady Metheraall
Saturday 13th July, 2019

Contents

Abstract	ii
Acknowledgements	iii
Author's Declaration	iv
Table of Contents	v
List of Figures	vii
List of Tables	ix
List of Acronyms	x
1 Introduction	1
1.1 Tuneable Lasers	3
1.1.1 Optical Coupler and Laser Output	4
1.1.2 Fibre Bragg Grating	5
1.1.3 Modulator	9
1.1.4 Optical Circulator	10
1.1.5 Optical Amplifier and Pump Laser	11
1.2 Mode-Locking	12
2 Previous Modelling Efforts	13
2.1 Nonlinear Optics	13
2.2 The Master Equation of Mode-Locking	15
2.3 Discrete Functional Models	17
3 A New Model	19
3.1 Components	19
3.1.1 Gain	20
3.1.2 Fibre Nonlinearity	21
3.1.3 Loss	22
3.1.4 Dispersion	23
3.1.5 Modulation	23
3.2 Non-Dimensionalization	24

3.3	Combining the Effects of Each Block of the Model	25
3.4	Solution to the Linear Model	26
3.4.1	Spread of the Pulse Due to Dispersion	28
3.4.2	Equilibrium Shape of the Pulse	31
3.4.3	Asymptotic Expansion of the Variance	32
3.4.4	Equilibrium Energy	39
3.5	Chapter Summary	41
4	Solution of the Nonlinear Model	43
4.1	Code	43
4.1.1	Validation	44
4.2	Nonlinear Model	46
4.2.1	Energy	49
4.2.2	Convergence	52
4.2.3	Permutation of Components	56
4.3	Chapter Summary	58
5	Conclusion	60
5.1	Future Work	61
References		63
A The Lambert W Function		70
B Span of Gaussians in $L^2(\mathbb{R})$		73
C Code		79

List of Figures

1.1	Depiction of a standard laser. A majority of the light is continually reflected by the two mirrors with a small portion escaping to become the output. The light is amplified by the gain medium with each pass.	1
1.2	Comparison of pumping, spontaneous emission, and stimulated emission.	2
1.3	Typical cavity of a tuneable laser.	4
1.4	Manufacture methods of fibre Bragg gratings.	6
1.5	Comparison of a chirped and unchirped Gaussian pulse.	7
1.6	Chirped fibre Bragg grating.	8
1.7	Symbol for a four port optical circulator.	10
1.8	Two examples of mode-locking.	12
3.1	Sample realization of (3.11).	27
3.2	Envelope, Fourier transform, and chirp of the pulse—linear case. . . .	33
3.3	Plot of (3.22) and (3.24) to highlight the structure.	34
3.4	Asymptotic expansion of the variance as the dispersion parameter approaches 0.	36
3.5	Asymptotic expansion of the variance as the dispersion parameter approaches ∞	38
4.1	Equilibrium variance, chirp, and phase shift of the pulse as a function of the dispersion parameter.	44
4.2	Equilibrium energy, and peak power of the pulse as a function of the dispersion parameter.	45
4.3	Envelope, Fourier transform, and chirp of the pulse—stable case. . . .	46
4.4	Rate of convergence as a function of number of iterations for various s values, with $b = 0.5$. The error is given by (4.1).	47
4.5	Energy of the pulse.	48
4.6	Stability of the pulse in the s - b plane.	49
4.7	Envelope, Fourier transform, and chirp of the pulse—unstable case. .	51
4.8	Error of the pulse envelope.	52
4.9	Error for various step sizes.	53
4.10	Composite error.	55
4.11	Energy of the pulse after 100 cycles with the modulation and dispersion blocks switched.	57

A.1	The two branches of the Lambert W function.	71
B.1	Two examples of Gaussian series.	76
B.2	Gaussian series for a particular modulation function.	77

List of Tables

3.1 Range of variation of various parameters.	25
---	----

List of Acronyms

CFBG chirped fibre Bragg grating. 7–9, 17, 23, 25, 27, 30, 32, 39, 56, 61

EDFA Erbium-doped fibre amplifiers. 11

FBG fibre Bragg grating. v, 5, 6, 11

FWHM full width at half maximum. 12, 27

GNLSE generalized nonlinear Schrödinger equation. 15

LED light emitting diode. 3

Nd:YAG Neodymium-doped Yttrium Aluminium garnet. 1

NLSE nonlinear Schrödinger equation. 14

SPM self-phase modulation. 18, 22, 44, 50, 58, 60

UV ultraviolet. 5, 6

WKB Wentzel–Kramers–Brillouin. 22

Introduction

The word laser was originally an acronym for *Light Amplification by Stimulated Emission of Radiation*. The cavity of a standard laser—such as a HeNe laser—is composed of four main components: a highly reflective mirror, a partially reflecting mirror, something to supply the energy, and the amplifying, or gain, medium. The two mirrors are at opposite ends of the cavity and serve to contain most of the light in the cavity while allowing a small amount to exit—this is the output of the laser, this is shown in Figure 1.1. The energy is generally supplied by either an external light source, or an electric field. The amplifying medium for a single frequency laser typically consists of gases, such as Helium and Neon, or a crystal, such as Neodymium-doped Yttrium Aluminium garnet (Nd:YAG).

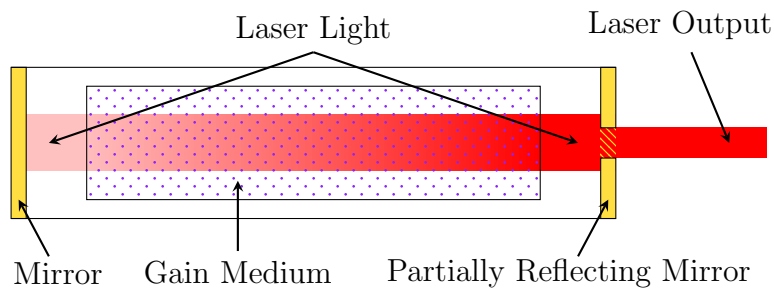


Figure 1.1: Depiction of a standard laser. A majority of the light is continually reflected by the two mirrors with a small portion escaping to become the output. The light is amplified by the gain medium with each pass.

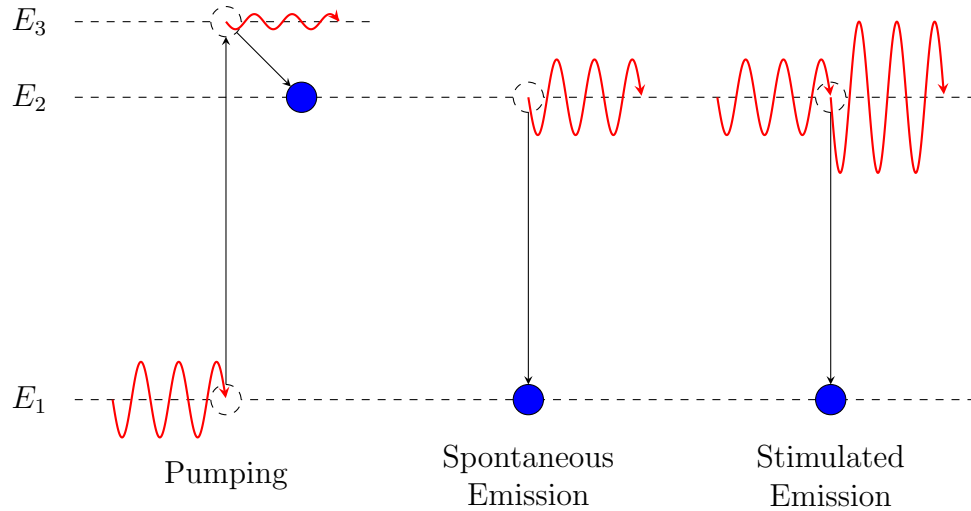


Figure 1.2: In pumping, incident photons are absorbed by electrons which are then excited into a much higher energy state (the electrons may also be excited by an electric field). The electrons quickly emit a low energy photon and transition down to an energy state that is still much more energetic than the original. In spontaneous emission, an electron in an excited state emits a photon and returns to the lower energy state. Finally, in stimulated emission, an incident photon interacts with an electron in an excited state, the electron donates its energy to the photon and returns to the lower energy state.

The atoms in the gain medium are pumped with energy raising the electrons to an excited state. For stimulated emission an incident photon triggers the emission of a photon which causes the electron to transition back to the ground state [1]. This new photon is emitted with the combined energy of the previous photon as well as the electron's energy, thus, amplifying the light. Furthermore, the photon is released with the same direction and phase as the incident one, maintaining coherence [1]. These processes are highlighted in Figure 1.2. The light perpetually bounces between the two mirrors becoming more amplified with each interaction with an excited electron and a fraction of this light is able to pass through the partially reflecting mirror to become the output of the laser.

Laser light has two fundamental characteristics that regular light does not. The

first is that the light is highly monochromatic—the light contains (ideally) a single frequency. This is in contrast with an incandescent light bulb, for example, which emits light at all wavelengths with relative intensities given by Planck’s law of black-body radiation. The other key feature is coherence, in which all the peaks and troughs of the light overlap giving very strong constructive interference—this is why laser light can be so intense. A system such as a [light emitting diode \(LED\)](#) does not produce laser light because, while monochromatic, the light is not coherent. The monochromatic nature is a result of how the light is generated; the frequency of the light emitted directly corresponds to the energy difference between the excited and ground states of the gain medium (as with [LEDs](#)). Note that this means the operating frequency of the laser is fixed, and cannot be changed. Coherence is achieved in the laser cavity—the cavity is carefully designed so the light resonates with the length of the cavity. This causes all the peaks and troughs to align, and interfere constructively.

Another class of lasers are optical fibre lasers. Optical fibre lasers operate by the same principles, however, instead of the light being perpetually reflected back and forth, the light travels in a circular fashion along an optical fibre—this is a so called ring laser. Additionally, instead of the gain medium consisting of a gas or crystal, it is a length of fibre doped with a rare-earth metal.

1.1 Tuneable Lasers

A tuneable laser has the ability to vary its wavelength, and hence frequency, by up to about 100 nanometres [2–4]. Tuneable lasers can lase at all of these different frequencies simultaneously. This tuneability is quite useful and has applications in spectroscopy and high resolution imaging such as coherent anti-Stokes Raman spec-

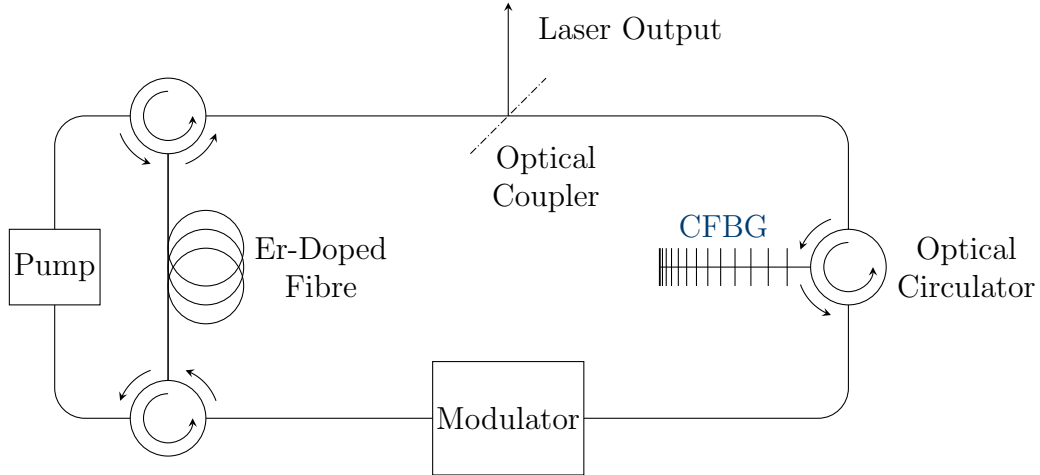


Figure 1.3: Typical cavity of a fibre based tuneable laser. The pulses travel clockwise around each loop.

troscopy and optical coherence tomography [2, 4, 5], as well as communications and diagnostics of ultra fast processes [6]. A typical tuneable laser cavity is shown in Figure 1.3. The gain medium is still excited by an external power source, and the output passes through a partially reflecting mirror. However, a tuneable laser also contains a few additional components, each of which will be described in the following subsections.

1.1.1 Optical Coupler and Laser Output

The optical coupler is a device that splits its input into two outputs—one continues through the laser cavity, while the other exits the cavity to become the output of the laser. There are multiple devices that can accomplish this, however, the simplest is a partially reflecting mirror [1]. These mirrors are characterized by their reflection coefficient, R . In the schematic shown in Figure 1.3, the part of the signal that is reflected exits the cavity, whereas the part of the signal transmitted remains within the cavity.

1.1.2 Fibre Bragg Grating

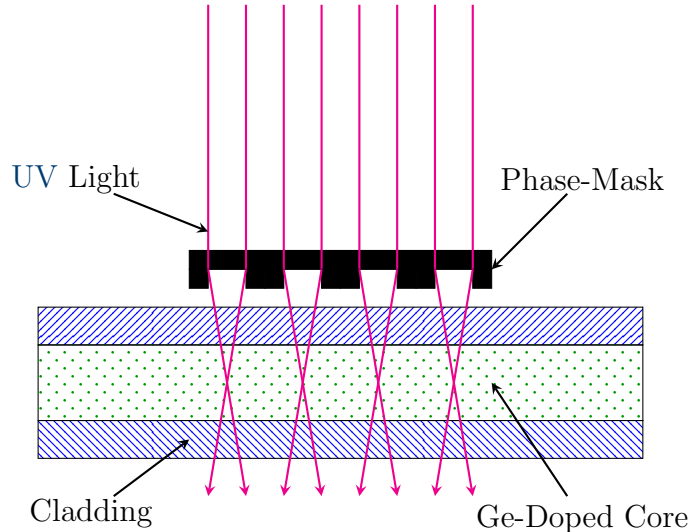
A fibre Bragg grating (FBG) is an optical fibre where the refractive index varies periodically along its length [7]. To achieve this periodicity, typically silica fibres are doped with Germanium which when exposed to intense **ultraviolet (UV)** light permanently alters the refractive index of the core [8,9]. The photosensitivity of the optical fibres can be increased by more than an order of magnitude by the Germanium doping [7,8].

FBGs can be manufactured using one of two methods—the phase-mask method [1,8–10], or the holographic side exposure method [1,7–10]—these are shown in Figure 1.4. Both methods cause the periodic nature of the refractive index through interference. In the phase-mask method (Figure 1.4a), a single beam of **UV** light passes through the phase-mask which acts as a series of lenses, focusing the light onto the core—this causes a sinusoidal interference pattern. Similarly, in the holographic side exposure method (Figure 1.4b), two beams of **UV** light are instead used to create the interference pattern.

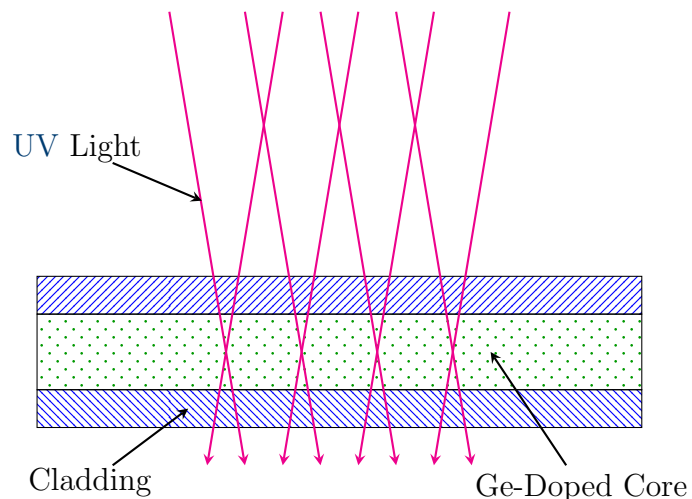
The purpose of FBGs is that they act as reflective filters [1,7,9,10]. Due to the periodicity of the refractive index, light with the corresponding wavelength will be reflected with all others passing through. This wavelength is defined by the Bragg condition [1,6–10]:

$$\lambda_B = 2\Lambda\bar{n}, \quad (1.1)$$

where λ_B is the Bragg wavelength, Λ is the period of the grating, and \bar{n} is the average index of refraction. Ideally, only light with a wavelength of λ_B would be reflected, however, there is a very narrow neighbourhood around λ_B in which wavelengths are



(a) **Phase-Mask:** The phase-mask refracts the **UV** light onto the core.



(b) **Holographic Side Exposure:** Two incident beams intersect at the core.

Figure 1.4: Depictions of the two most common methods for manufacturing **FBGs**. The **UV** light is focused on the core causing periodic constructive and destructive interference. The **UV** light alters the refractive index of the core, causing a sinusoidal variation along the length.

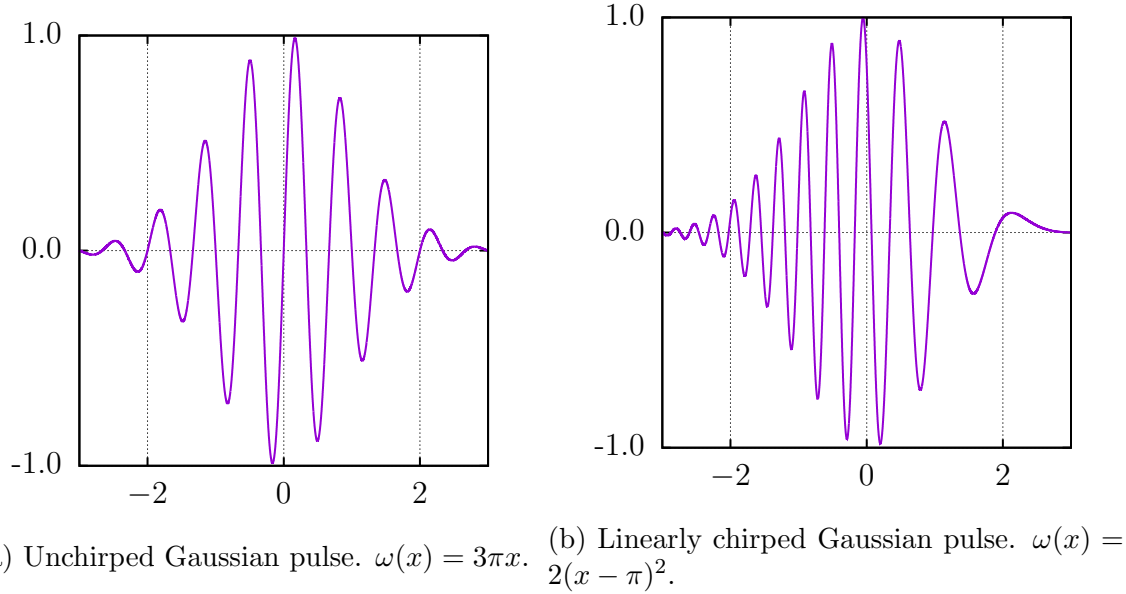


Figure 1.5: In an unchirped pulse the frequency is constant, however, in a chirped pulse the frequency varies along the envelope. The waveforms are given by $\exp(-x^2/2) \sin \omega(x)$.

partially reflected too; the characteristic width of this region is known as the stop-band.

Chirped Fibre Bragg Grating

Chirp is simply the term for a signal that has a non-constant frequency across it. Figure 1.5 shows examples of chirped and unchirped Gaussian pulses—the most common type of chirp is linear chirp, where the frequency varies linearly across the pulse. In this case, for a spatially varying frequency, the oscillations are characterized by $\exp(ik(x)x) = \exp(iCx^2)$, where $k(x) = Cx$ is the linear variation of the wave number, and C is the chirp parameter. By using a chirped phase-mask, a **chirped fibre Bragg grating (CFBG)** can be created. The spacial variation of the refractive index effectively creates a spacial dependence on the Bragg condition, (1.1). This causes most wavelengths to be reflected by a CFBG, but with each wavelength satisfying the

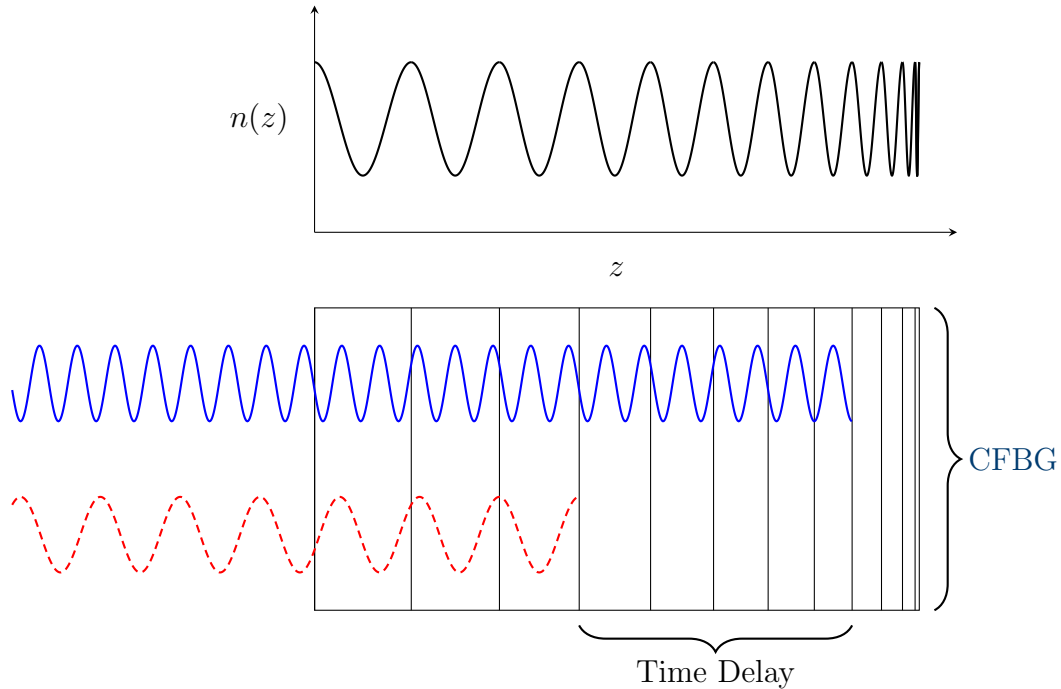


Figure 1.6: **Chirped fibre Bragg grating**. The upper portion shows how the index of refraction varies along the depth. Light is reflected when the wavelength coincides with the Bragg wavelength. This causes light with different wavelengths to penetrate to different depths. In turn, dispersion is either heightened or compensated—depending on the orientation.

Bragg condition at a different spacial location¹. A consequence of this is that a time delay is created between wavelengths—this is depicted in Figure 1.6 with the upper portion showing the refractive index as a function of the depth. In this orientation, the red (dashed) wave is unable to penetrate as far as the blue (solid) wave since each wave is reflected where it matches the frequency of the refractive index. Each CFBG has a bandwidth within which all frequencies are reflected at some point along the depth, alternatively, frequencies outside the bandwidth would be transmitted and lost.

Furthermore, the speed of light in an optical fibre is slightly dependent on the wavelength—this causes light with a longer wavelength to travel faster, and is known as chromatic dispersion. This is a large problem in fibre optic communications, the

¹Note that a monotonic chirping ensures that the spacial dependence of the Bragg condition is continuous with respect to the wavelength.

signal can spread and potentially becomes unrecoverable after vast distances. However, chromatic dispersion can be counteracted using a CFBG [1,8–10] (in the opposite orientation of Figure 1.6). By forcing the longer wavelengths to travel farther the dispersion can be reversed, restoring the original signal. In one experiment [11], a signal was successfully transmitted over 109 km at 40 Gb/s by compensating the dispersion with two 40 cm CFBGs. Over this distance, the pulse would have spread to about 55 times its original width, and could only have been transmitted 4 km at that bit rate. At reduced bit rates however, a 10 cm CFBG can compensate the dispersion of 300 km of fibre [10]. However, in our case, we wish to control the dispersion, simulating hundreds of metres of fibre, so the CFBG is used in the orientation shown in Figure 1.6.

1.1.3 Modulator

The modulator serves the purpose of reshaping the pulse. Without it, the pulse will repeatedly widen due to the CFBG, but the modulator ensures the pulse is band limited by altering the envelope. The optical pulse in the cavity can be modulated with one of two methods—amplitude modulation, or phase modulation. Mathematically these can be considered equivalent since they are Fourier transforms of each other, but in practice these are accomplished by different apparatuses. We shall assume the pulses are amplitude modulated to minimize the analysis required in the Fourier domain. Generally, the pulse can be amplitude modulated using one of two techniques. The first is with an acousto-optic modulator which utilizes the acousto-optic effect where the index of refraction of the optical fibre is varied by a sound wave [12,13]. The second—and more common—method uses the electro-optic effect, where the index of refraction of the optical fibre is varied by an electric field, and is called an electro-optic modulator. This modulator works the same was as an acousto-optic modulator,

the optical fibre inside the modulator responds to an applied electric field, modifying the index of refraction [10, 12–14]. The shape of the electrical (sound) pulse can be controlled in such a way to provide the desired effect of modulation.

A Mach–Zehnder interferometer can be used in tandem with an acousto- or electro-optic modulator to modulate an optical pulse. The incident pulse is separated with a Y-waveguide, one of the two branches is then modulated, and finally the two branches are recombined with another Y-waveguide [1, 12, 13]. In the absence of a modulator on one of the branches the two pulses recombine into the original pulse. However, with modulation the two pulses are no longer identical, and so when the recombine, they interfere. This interference can be used to further modulate the pulse [10, 12, 13, 15].

1.1.4 Optical Circulator

An optical circulator is a device that routes signals from port to port in a circular fashion [1, 8, 10], the symbol for a four port optical circulator is shown in Figure 1.7. While a four port optical circulator is most common, within Figure 1.3 only three port optical circulators are required. A signal entering from port 1 will be outputted to port 2; a signal en-

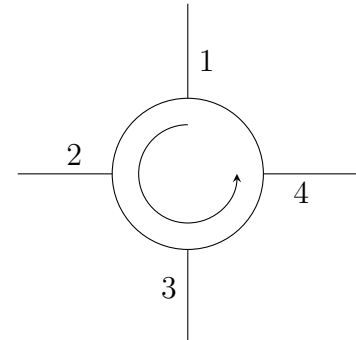


Figure 1.7: Symbol for a four port optical circulator.

tering from port 2 will exit from port 3; and so forth. Typically, optical circulators have three or four ports, with the first port being input only, and the final port being output only [1]. Optical circulators are most commonly used with devices that reflect signals instead of transmit them. For example, a signal may enter through port 1,

exit through port 2, be reflected by an FBG, re-enter port 2, and finally exit through port 3.

1.1.5 Optical Amplifier and Pump Laser

Optical amplifiers are of particular importance in fibre optic communications, they are used to restore the strength of a signal after it has been attenuated over large distances, or when a signal is divided into multiple paths [1, 9]. They are also more efficient, and introduce less noise than an electrical repeater. In this context, the optical amplifier provides the energy of the laser [1]. Most commonly, optical amplifiers are created by doping a length of fibre (called the gain fibre) with a rare-earth element which receives power from a pump laser [1, 9, 10]. The most common dopant is Erbium, however, Ytterbium and Neodymium are also used. Holmium, Samarium, Thulium, and Tellurium are infrequently used as well [10].

Erbium-doped fibre amplifiers (EDFA) are used most widely since the Erbium-doped fibre has a band gap that corresponds to 1.54–1.57 μm , which is the preferred band for fibre optics since this has the least power loss [1, 9, 10]. The pump laser typically operates at 980 nm or 1480 nm because these wavelengths are able to transfer the most power (up to 100 mW) into the fibre while introducing minimal noise [1, 8–10]. The pump power can be applied either forwards (with the laser), backwards (against the laser), or both [1], with each configuration having similar performance [10]. However, backwards pumping has slightly better performance at high powers when the gain begins to saturate² [10]. Additionally, with the configuration shown in Figure 1.3, the optical circulators can be used to isolate the pump circuit from the rest of the laser cavity.

²This concept will be discussed in Section 3.1.1.

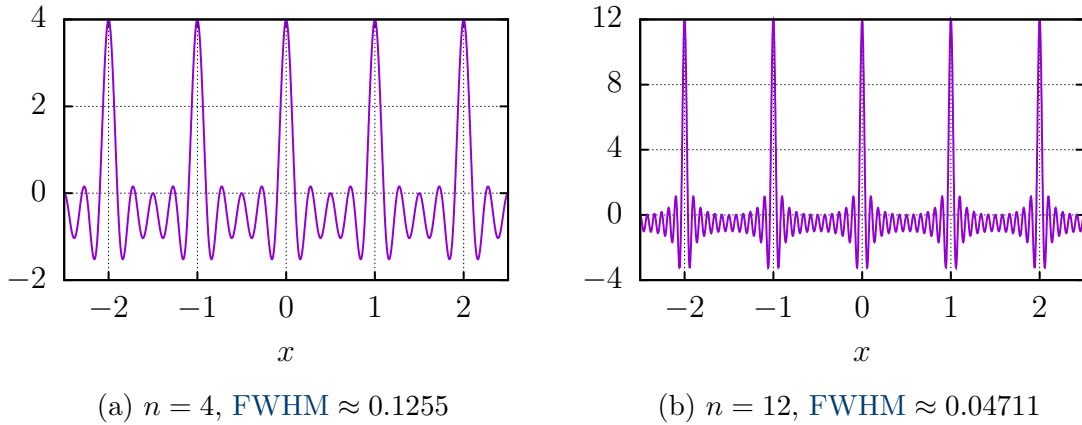


Figure 1.8: Two examples of mode-locking given by $\sum_{k=1}^n \cos(2\pi kx)$.

1.2 Mode-Locking

Recall, one of the fundamental features of a laser is coherence. However, in the context of tuneable lasers it is perhaps less clear what is meant by coherence since the light is no longer monochromatic. Instead, we have a particular peak of all the frequencies aligned, that is, the phase shift between modes is zero. This process is called mode-locking—all of the different modes are locked together at a peak [6, 12, 15]. This of course creates a very intense and short pulse of light—as short as 5 fs [6]. At this particular peak all of the frequencies constructively interfere as with a standard laser, however, deviations from the peak lead to destructive interference. Two examples of this are shown in Figure 1.8, and as expected, including more modes simultaneously narrows and intensifies the pulse.

2

Chapter

Previous Modelling Efforts

In this chapter we shall explore the previous modelling efforts by first reviewing the classic equations used in nonlinear optics. We will then build upon this to obtain the master equation of mode-locking, the solutions to this will briefly be reviewed before considering discretized functional models.

2.1 Nonlinear Optics

The standard equation for studying nonlinear optics—which can be derived from the nonlinear wave equation for electric fields¹—is

$$\frac{\partial A}{\partial z} = -i \frac{\beta_2}{2} \frac{\partial^2 A}{\partial t^2} + i\gamma|A|^2 A - \frac{1}{v_g} \frac{\partial A}{\partial t}. \quad (2.1)$$

Here $A = A(z, t) : \mathbb{R}^2 \mapsto \mathbb{C}$ is the complex pulse amplitude, $\beta_2 \in \mathbb{R}$ is the second order—or group delay—dispersion, $\gamma \in \mathbb{R}$ is the coefficient of nonlinearity or Kerr coefficient, and $v_g \in \mathbb{R}^+$ is the group velocity. However, it is customary to transform

¹The derivation is presented in detail in [7, 15].

(2.1) into a comoving reference frame, this is achieved with the substitution

$$T = t - \frac{z}{v_g}, \quad (2.2)$$

reminiscent of moving to a fixed frame in a free boundary problem [16]. Now, $\frac{\partial}{\partial t} \mapsto \frac{\partial}{\partial T}$, and $\frac{\partial}{\partial z} \mapsto \frac{\partial}{\partial z} - \frac{1}{v_g} \frac{\partial}{\partial T}$ by chain rule. Under this transformation, z still defines the distance travelled by the pulse, but, T now designates the time difference from the peak of the pulse for a given z . Moreover, $T < 0$ is the leading edge of the pulse, and $T > 0$ is the trailing edge regardless of the actual time elapsed, and because of this, generally T is not very large. Furthermore, the substitution (2.2) cancels the final term of (2.1), yielding

$$\frac{\partial A}{\partial z} = -i \frac{\beta_2}{2} \frac{\partial^2 A}{\partial T^2} + i\gamma |A|^2 A. \quad (2.3)$$

Despite being physically unrelated to quantum mechanics (2.3) is called the **nonlinear Schrödinger equation (NLSE)** because of its functional similarity [7, 15, 17–21].

The β_2 term comes from a Taylor expansion of the wavenumber [22], that is,

$$\begin{aligned} k(\omega) &= k_0 + \left. \frac{\partial k}{\partial \omega} \right|_{\omega_0} (\omega - \omega_0) + \frac{1}{2} \left. \frac{\partial^2 k}{\partial \omega^2} \right|_{\omega_0} (\omega - \omega_0)^2 + \frac{1}{6} \left. \frac{\partial^3 k}{\partial \omega^3} \right|_{\omega_0} (\omega - \omega_0)^3 + \dots \\ &= k_0 + \frac{1}{v_g} (\omega - \omega_0) + \frac{1}{2} \beta_2 (\omega - \omega_0)^2 + \frac{1}{6} \beta_3 (\omega - \omega_0)^3 + \dots, \end{aligned}$$

where ω_0 is the central frequency of operation, $k_0 = k(\omega_0)$, and β_3 is the third order dispersive effects. Typically, these third order effects must only be considered for ultrashort pulses—pulse widths less than ~ 5 ps—because of their large bandwidth [15], or a highly dispersive media [15, 23]. However, for simplicity and because of the nature of the grating, the third order effects can be neglected [7, 15].

In practice, (2.3) lacks a few key terms. Thus, it is often generalized by adding amplification, loss, and occasionally higher order terms. This gives the [generalized nonlinear Schrödinger equation \(GNLSE\)](#) [2, 15, 20, 24–26],

$$\frac{\partial A}{\partial z} = -i\frac{\beta_2}{2}\frac{\partial^2 A}{\partial T^2} + i\gamma|A|^2A + \frac{1}{2}g(A)A - \alpha A, \quad (2.4)$$

where $g(A)$ is an amplifying term due to the gain, and $\alpha \in \mathbb{R}$ is the loss due to scattering and absorption.

2.2 The Master Equation of Mode-Locking

The [GNLSE](#) has many applications in nonlinear optics and fibre optic communications, however, in the context of lasers we wish to add a modulation term to ensure mode-locking, this yields the master equation of mode-locking, [12, 22, 27–32]

$$\frac{\partial A}{\partial z} = -i\frac{\beta_2}{2}\frac{\partial^2 A}{\partial T^2} + i\gamma|A|^2A + \frac{1}{2}g(A)A - \alpha A - M(T). \quad (2.5)$$

The most common form of modulation is the sinusoid $M(T) = \frac{1}{2}\frac{M_s}{\omega_M^2}(1 - \cos(\omega_M T))$ [12, 22, 27, 33], where M_s is the strength of modulation and ω_M is the frequency of modulation. Moreover, since T is generally small, we expand via Taylor series so that $M(T) = \frac{1}{2}M_sT^2 + \mathcal{O}(T^4)$. This brings us to the most common form of the master equation of mode-locking,

$$\frac{\partial A}{\partial z} = -i\frac{\beta_2}{2}\frac{\partial^2 A}{\partial T^2} + i\gamma|A|^2A + \frac{1}{2}g(A)A - \alpha A - \frac{1}{2}M_sT^2. \quad (2.6)$$

Commonly, in an attempt to simplify the equation, the gain is assumed to be constant with $g(A) = 2g_0 \in \mathbb{R}$. No analytic solution is known for (2.6), however, after

additional simplifications there are three types of solutions.

In the least complicated case, the modulation and nonlinearity are both omitted giving

$$\frac{\partial A}{\partial z} = -i \frac{\beta_2}{2} \frac{\partial^2 A}{\partial T^2} + (g_0 - \alpha)A. \quad (2.7)$$

This results in a solution in the form of a hyperbolic secant [27–29]. On the other hand, including the nonlinearity yields

$$\frac{\partial A}{\partial z} = -i \frac{\beta_2}{2} \frac{\partial^2 A}{\partial T^2} + i\gamma|A|^2A + (g_0 - \alpha)A, \quad (2.8)$$

where a similar solution is found, however, it is instead of the form of a chirped hyperbolic secant [32,34]. The nature of the solutions to (2.7) and (2.8) is as expected. These equations are slight generalizations of (2.3) which has a soliton solution of a hyperbolic secant [7]. Finally, by including the modulation term, and excluding the nonlinearity we have

$$\frac{\partial A}{\partial z} = -i \frac{\beta_2}{2} \frac{\partial^2 A}{\partial T^2} + (g_0 - \alpha)A - \frac{1}{2}M_sT^2. \quad (2.9)$$

This can be solved using separation of variables and one finds the solutions are the Gaussian–Hermite polynomials [5, 12, 22, 27, 30–33], defined recursively as

$$\tilde{H}_n(x) := (-1)^n e^{x^2/2} \frac{d^n}{dx^n} e^{-x^2}, \quad (2.10)$$

However, in practice only the Gaussian is stable—the higher modes quickly decay within the laser [12, 27, 30, 33]. For a more comprehensive history see [30].

2.3 Discrete Functional Models

While the derivation of (2.6) is correct mathematically, it is not representative of what happens within the laser cavity. The issue with (2.6) is that it has been assumed each process affects the pulse continuously within the cavity. As highlighted by Figure 1.3, this is a rather poor assumption. Within the cavity each effect is localized to its corresponding component: almost all of the dispersion happens within the CFBG, the pulse is only amplified within the Erbium-doped fibre, etc. Thus, perhaps a better model is one where (2.6) is broken down into the individual components giving the effect of each ‘block’ of the cavity. Each of the blocks can then be composed together to give an iterative map for the effect of one circuit around the cavity. This yields an algebraic equation instead of a differential one.

Such a method was first proposed in 1955 by Cutler [35] while analyzing a microwave regenerative pulse generator. This method was adapted for mode-locked lasers in 1969 by Siegman and Kuizenga [36, 37]. Kuizenga and Siegman also had success experimentally validating their model [38, 39]. The effects of the nonlinearity would not be considered until Martinez, Fork, and Gordon [40, 41] tried modelling passive mode-locking—mode-locking without the use of a modulator. In the absence of a modulator the nonlinearity becomes crucial to shaping the pulse. This issue has recently been readdressed by Burgoyne [5] in the literature for tuneable lasers. In these models the effect of each block is described by a transfer function, for example:

$$A_{\text{out}}(T) = A_{\text{in}}(T) \exp\left(-\frac{\epsilon T^2}{2}\right) e^{i\phi_M - \alpha_M/2},$$

$$\widehat{A}_{\text{out}}(\Omega) = \widehat{A}_{\text{in}}(\Omega) \exp\left(\frac{i\beta_2 \Omega^2}{2}\right) e^{i\phi_D - \alpha_D/2},$$

for modulation and dispersion, respectively. These transfer functions are then mul-

tiplied together to give the overall effect. This is in contrast to the iterative map developed in Sections 3.1–3.3.

Despite the development of block style models, several short-comings exist. The clearest is that none of these models have contained every block—either the nonlinearity or the modulation have been omitted. In the framework of tuneable lasers, each component plays a crucial role and the tuneable laser will not function without the inclusion of all of the components. Another key drawback is that the functional operations of some of the components used in other models are somewhat phenomenological. While these functions are chosen based on the observed output, they are not necessarily consistent with their underlying physics. Finally, none of these previous models have been able to exhibit a phenomena called *wave-breaking* in which the self-phase modulation of the pulse becomes too strong, distorting and damaging the wave until it ultimately becomes unstable and unsustainable. This notion will be explored in greater detail in Chapter 4.

Chapter 3

A New Model

In this chapter we shall derive our new model and solve it analytically in the linear case. To accomplish this we shall use the ideas of the previous functional models [5, 35–41]. To alleviate some of the pitfalls mentioned in the previous chapter, we shall include all five processes involved in the modification of the pulse within the laser cavity (gain, nonlinearity, loss, dispersion, and modulation). In addition to this, the functional operations associated with each component will be derived from (2.4), with the exception of the modulation in which we consider the exact functional form to be determined by the laser operator.

3.1 Components

We shall begin our analysis with the derivation of the functional operators for the five components.

3.1.1 Gain

Within the Er-doped gain fibre, the gain term is dominant, and equation (2.4) reduces to

$$\frac{\partial A}{\partial z} = \frac{1}{2}g(A)A, \quad (3.1)$$

where $g(A)$ takes the form [2, 5, 6, 12, 22, 24–27, 29, 30, 32, 34]

$$g(A) = \frac{g_0}{1 + E/E_{\text{sat}}}, \quad E = \int_{-\infty}^{\infty} |A|^2 dT, \quad (3.2)$$

where g_0 is a small signal gain, E is the energy of the pulse, and E_{sat} is the energy at which the gain begins to saturate. Multiplying (3.1) by \bar{A} , the complex conjugate of A , yields

$$\bar{A} \frac{\partial A}{\partial z} = \frac{1}{2} \frac{g_0 |A|^2}{1 + E/E_{\text{sat}}},$$

adding this to its complex conjugate gives

$$\frac{\partial |A|^2}{\partial z} = \frac{g_0 |A|^2}{1 + E/E_{\text{sat}}}. \quad (3.3)$$

After integrating this becomes

$$\frac{dE}{dz} = \frac{g_0 E}{1 + E/E_{\text{sat}}}. \quad (3.4)$$

For $E \ll E_{\text{sat}}$ the energy will grow exponentially, whereas for $E \gg E_{\text{sat}}$ the gain has saturated and so the growth is linear. To obtain a closed form solution, (3.4) is integrated over a gain fibre of length L_g , the length of the gain fibre, and assuming

the energy increases from E to E_{out} , then

$$g_0 L_g = \log \frac{E_{\text{out}}}{E} + \frac{E_{\text{out}} - E}{E_{\text{sat}}},$$

and by exponentiating, rearranging, and applying W , the Lambert W function¹,

$$W\left(\frac{E}{E_{\text{sat}}} e^{E/E_{\text{sat}}} e^{g_0 L_g}\right) = W\left(\frac{E_{\text{out}}}{E_{\text{sat}}} e^{E_{\text{out}}/E_{\text{sat}}}\right) = \frac{E_{\text{out}}}{E_{\text{sat}}},$$

by (A.1). This results in the closed form expression

$$E_{\text{out}} = E_{\text{sat}} W\left(\frac{E}{E_{\text{sat}}} e^{E/E_{\text{sat}}} e^{g_0 L_g}\right).$$

Notice from (3.3) and (3.4) that

$$\frac{1}{|A|^2} \frac{\partial |A|^2}{\partial z} = \frac{1}{E} \frac{dE}{dz}$$

and so, $E \sim |A|^2$, therefore the gain in terms of the amplitude is given by

$$G(A; E) = \left(\frac{E_{\text{out}}}{E}\right)^{1/2} A = \left(\frac{E_{\text{sat}}}{E} W\left(\frac{E}{E_{\text{sat}}} e^{E/E_{\text{sat}}} e^{g_0 L_g}\right)\right)^{1/2} A$$

after passing through the gain fibre once.

3.1.2 Fibre Nonlinearity

The nonlinearity of the fibre arises from the parameter γ ; in regions where this effect is dominant expression (2.4) becomes

$$\frac{\partial A}{\partial z} - i\gamma |A|^2 A = 0. \quad (3.5)$$

¹See Appendix A.

This expression can be manipulated in a similar manner to the gain to show $\frac{\partial}{\partial z}|A|^2 = 0$, suggesting the WKB ansatz $A(z, T) = A_0(T)e^{i\varphi(T, z)}$. Substituting this representation into (3.5) and setting $\varphi(T, 0) = 0$ gives $\varphi(T, z) = \gamma|A|^2z$. For a fibre of length L_f the effect of the nonlinearity is given by the map $A \mapsto F(A)$, where

$$F(A) = Ae^{i\gamma|A|^2L_f}.$$

This is also frequently called the Kerr nonlinearity or Kerr effect after John Kerr who discovered the effect in 1875. As we shall see in Section 4.2.1, this is what is responsible for self-phase modulation and ultimately the degradation of the pulse [19, 31, 40, 42].

3.1.3 Loss

Two sources of loss exist within the laser circuit: the loss due to the output coupler and the optical loss due to absorption and scattering. The first case is simply a scalar multiplication depending on the reflectivity of the output coupler. The loss due to absorption and scattering can be derived from (2.4),

$$\frac{\partial A}{\partial z} = -\alpha A,$$

and gives $e^{-\alpha L_T} A$, which by multiplying by the amount of the signal lost to the output coupler gives

$$L(A) = (1 - R)e^{-\alpha L_T} A,$$

where R is the reflectivity of the output coupler, and L_T is the total length of the laser circuit as the effect of the losses².

²Depending on the experimental setup the loss may take the form $L(A) = Re^{-\alpha L_T} A$.

3.1.4 Dispersion

Within the laser cavity, the dispersion is dominated by the CFBG. In comparison, the dispersion due to the fibre is negligible. The dispersive terms of (2.4) give

$$\frac{\partial A}{\partial z} = -i \frac{\beta_2}{2} \frac{\partial^2 A}{\partial T^2}, \quad (3.6)$$

and since dispersion acts in the frequency domain it is convenient to take the Fourier transform³ of (3.6) [43, 44], giving

$$\frac{\partial}{\partial z} \mathcal{F}\{A\} = i \frac{\omega^2}{2} \beta_2 \mathcal{F}\{A\}.$$

The effect of dispersion is then given by the map

$$D(A) = \mathcal{F}^{-1} \left\{ e^{i\omega^2 L_D \beta_2 / 2} \mathcal{F}\{A\} \right\},$$

where L_D is the length of the dispersive medium.

3.1.5 Modulation

In (2.6), the amount of modulation is characterized by the parameter M_s through the term $\frac{1}{2} M_s T^2 A$. In this new model, the modulation is considered to be applied externally through its action on the spectrum. For simplicity the representation is taken as the Gaussian

$$M(A) = e^{-T^2 / 2T_M^2} A,$$

³We use $\mathcal{F}\{f\} = (2\pi)^{-1/2} \int_{\mathbb{R}} f(x) e^{i\omega x} dx$ as the definition of the Fourier transform.

where T_M is a characteristic width of the modulation.

Despite assuming a Gaussian modulation, the solution presented in Section 3.4 can be generalized to any modulation function in $L^2(\mathbb{R})$ since Gaussians in fact span $L^2(\mathbb{R})$ as shown in Appendix B.

3.2 Non-Dimensionalization

The structure of each process of the laser can be better understood by re-scaling the time, energy, and amplitude. Nominal values for tuneable lasers are shown in Table 3.1. Knowing experimental durations and energies, the table suggests the convenient scalings:

$$T = T_M \tilde{T}, \quad E = E_{\text{sat}} \tilde{E}, \quad A = \left(\frac{E_{\text{sat}}}{T_M} \right)^{1/2} \tilde{A}. \quad (3.7)$$

Revisiting each process map shows each process has a characteristic non-dimensional parameter. The new mappings, after dropping the tildes, are

$$G(A) = (E^{-1} W(a E e^E))^{1/2} A, \quad (3.8a)$$

$$F(A) = A e^{ib|A|^2}, \quad (3.8b)$$

$$L(A) = h A, \quad (3.8c)$$

$$D(A) = \mathcal{F}^{-1} \left\{ e^{is^2 \omega^2} \mathcal{F}\{A\} \right\}, \quad (3.8d)$$

$$M(A) = e^{-T^2/2} A, \quad (3.8e)$$

Parameter	Symbol	Value	Sources
Absorption of Fibre ⁴	α	10^{-4} – 0.3 m^{-1}	[25, 26, 32, 45, 46]
Fibre Dispersion	β_2^f	-50 – $50 \text{ ps}^2/\text{km}$	[5, 10, 15, 23, 24, 26]
Fibre Nonlinearity	γ	0.001 – $0.01 \text{ W}^{-1}\text{m}^{-1}$	[15, 20, 26, 32]
Grating Dispersion	$\beta_2^g L_D$	10 – 2000 ps^2	[5, 10, 15, 47]
Length of Cavity	L_T	10 – 100 m	[24, 31, 45]
Length of Fibre	L_f	0.15 – 1 m	[45]
Length of Gain Fibre	L_g	2 – 3 m	[5, 24–26, 48]
Modulation Time	T_M	15 – 150 ps	[2, 5, 45]
Reflectivity of Optical Coupler	R	0.1 – 0.9	[4, 24, 31, 45, 47, 48]
Saturation Energy	E_{sat}	10^3 – 10^4 pJ	[26, 32, 45]
Small Signal Gain	g_0	1 – 10 m^{-1}	[26, 45]

Table 3.1: Range of variation of various parameters.

with the four dimensionless parameters, as defined by the values in Table 3.1,

$$\begin{aligned} a &= e^{g_0 L_g} \sim 8 \times 10^3, & h &= (1 - R)e^{-\alpha L} \sim 0.04, \\ b &= \gamma L_f \frac{E_{\text{sat}}}{T_M} \sim 1, & s &= \sqrt{\frac{\beta_2 L_D}{2 T_M^2}} \sim 0.2, \end{aligned} \quad (3.9)$$

which characterize the behaviour of the laser. Notice that the modulation is characterized by T_M , and each other process has its own independent non-dimensional parameter.

3.3 Combining the Effects of Each Block of the Model

In this model the pulse is iteratively passed through each process, the order of which must now be considered. We are most interested in the output of the laser cavity, and so we shall start with the loss component. Next the pulse is passed through the CFBG, as well as the modulator. Finally, the pulse travels through the gain fibre to be amplified, and then we consider the effect of the nonlinearity since this is the

⁴Fibre loss is typically reported as $\sim 0.5 \text{ dB/km}$.

region where the power is maximized. Note that in general the functional operators of the components do not commute, and therefore the order of the components is indeed important—in contrast to the previous models. This is especially the case of dispersion as realized through the Fourier transform. The pulse after one complete circuit of the laser cavity is then passed back in to restart the process. Functionally this can be denoted as

$$\mathcal{L}(A) = F(G(M(D(L(A))))), \quad (3.10)$$

where \mathcal{L} is one loop of the laser. A steady solution to this model is one in which the envelope and chirp are unchanged after traversing every component in the cavity, that is, such that $\mathcal{L}(A) = Ae^{i\phi}$ —for some $\phi \in \mathbb{R}$. The phase shift is allowable because it is immeasurable in the laboratory—only the envelope, chirp, and variance can be measured.

3.4 Solution to the Linear Model

In reality the nonlinearity parameter, b , is of order unity by (3.9), but we shall start our investigation with the simpler case of $b = 0$ —which shall be referred to as the linear model. In this case, a solution can be found analytically. It is expected the solution will take the form of a Gaussian. There are a few reasons for this; the solution to the previous models were Gaussian [35–37, 40, 41] (see Section 2.2), the equilibrium shape will be highly correlated to the shape of the modulation function, and since a Gaussian is a fixed point of the Fourier transform [44] dispersion will not alter the envelope.

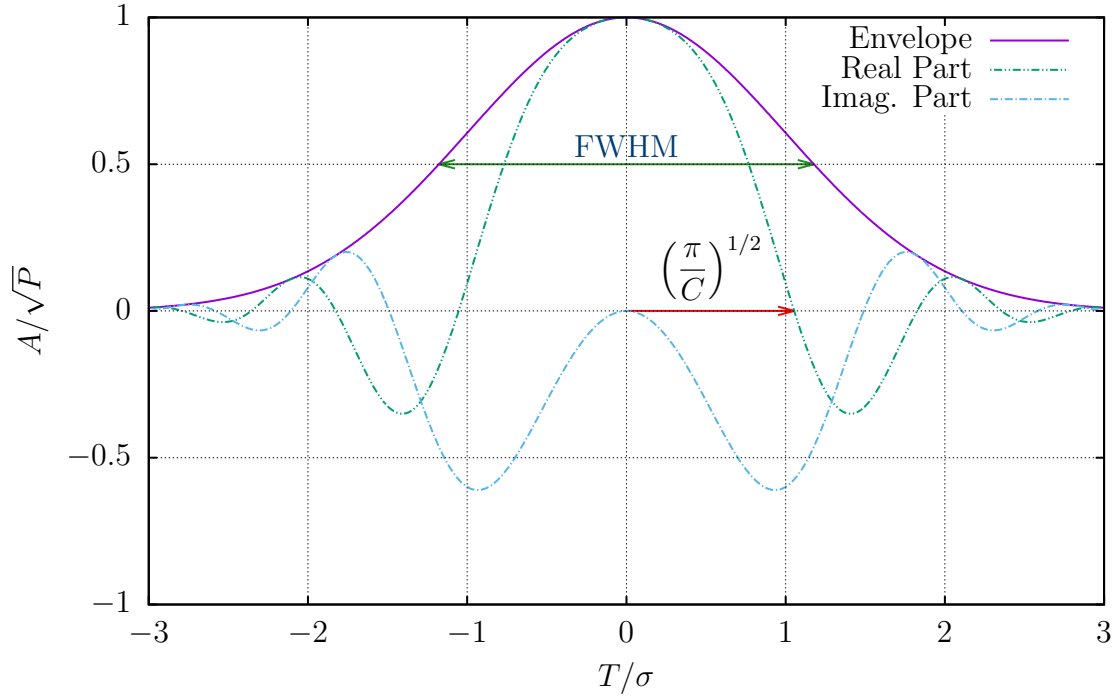


Figure 3.1: Sample realization of (3.11).

To compute $\mathcal{L}(A)$, consider the initial pulse

$$A_0 = \sqrt{P} \exp\left(-(1+iC)\frac{T^2}{2\sigma^2}\right) e^{i\phi_0}, \quad (3.11)$$

where P is the peak power, C is the chirp⁵, σ^2 is the variance, and ϕ_0 is the initial phase. An example of such a pulse is shown in Figure 3.1. This form is chosen because it matches the envelope and linear chirping found by experiment. After passing through the optical coupler the pulse will simply decay to $A_1 = L(A_0) = hA_0$. The pulse then enters the CFBG, where it will maintain its Gaussian shape, however, it will spread [6, 7, 15]. This can be written as

$$A_2 = D(A_1) = \sqrt{Ph\zeta} \exp\left(-(1+i\tilde{C})\frac{T^2}{2\tilde{\sigma}^2}\right) e^{i(\phi_0+\phi)}, \quad (3.12)$$

where $\tilde{\sigma}^2$ denotes the resulting variance, \tilde{C} denotes the resulting chirp, ζ is the re-

⁵As discussed in Section 1.1.2.

duction of the amplitude caused by the spread, and ϕ is the inherited phase shift from dispersion. At this point $\tilde{\sigma}^2$, \tilde{C} , ζ , and ϕ remain undetermined, and are used as placeholders for convenience. Next, the pulse is modulated:

$$A_3 = M(A_2) = \sqrt{P}h\zeta \exp\left(-(1+i\tilde{C})\frac{T^2}{2\tilde{\sigma}^2} - \frac{T^2}{2}\right) e^{i(\phi_0+\phi)}. \quad (3.13)$$

Finally, the pulse travels through the gain fibre where it is amplified to

$$A_4 = G(A_3) = \mathcal{L}(A_0) = \sqrt{P}\left(\frac{W(aEe^E)}{E}\right)^{1/2} h\zeta \exp\left(-(1+i\tilde{C})\frac{T^2}{2\tilde{\sigma}^2} - \frac{T^2}{2}\right) e^{i(\phi_0+\phi)}, \quad (3.14)$$

with E the energy of the pulse as it enters the gain fibre.

In equilibrium it must be that $A_0 = A_4 e^{-i\phi} = \mathcal{L}(A_0) e^{-i\phi}$ so that after a single loop of the cavity the variance, chirp, and envelope remain unchanged. More explicitly, this gives three conditions:

$$1 = \left(\frac{W(aEe^E)}{E}\right)^{1/2} h\zeta, \quad (3.15a)$$

$$\frac{1}{\sigma^2} = \frac{1}{\tilde{\sigma}^2} + 1, \quad (3.15b)$$

$$\frac{C}{\sigma^2} = \frac{\tilde{C}}{\tilde{\sigma}^2}. \quad (3.15c)$$

3.4.1 Spread of the Pulse Due to Dispersion

Each of these processes has a relatively straight forward effect, with the exception of dispersion. The effect of dispersion can be computed analytically for input pulses

using (3.8d). In the case of a Gaussian pulse, we make use of the transforms [43, 44]

$$\mathcal{F}\left\{e^{-\eta T^2}\right\} = (2\eta)^{-1/2} e^{-\omega^2/4\eta}, \quad \mathcal{F}^{-1}\left\{e^{-\eta\omega^2}\right\} = (2\eta)^{-1/2} e^{-T^2/4\eta}.$$

From (3.8d) we have that

$$\begin{aligned} D\left(e^{-\eta T^2}\right) &= \mathcal{F}^{-1}\left\{e^{is^2\omega^2} \mathcal{F}\left\{e^{-\eta T^2}\right\}\right\}, \\ &= (2\eta)^{-1/2} \mathcal{F}^{-1}\left\{\exp\left(-\omega^2\left(\frac{1}{4\eta} - is^2\right)\right)\right\}, \\ &= (1 - 4i\eta s^2)^{-1/2} \exp\left(-T^2 \frac{a}{1 - 4is^2\eta}\right). \end{aligned}$$

For us, $\eta = \frac{1}{2} \frac{1+iC}{\sigma^2}$; making this substitution yields

$$D(A_1) = \left(1 + \frac{2Cs^2}{\sigma^2} - \frac{2s^2}{\sigma^2}i\right)^{-1/2} \exp\left(-T^2 \frac{1+iC}{2\sigma^2 - 4is^2(1+iC)}\right).$$

This can be greatly simplified by first rationalizing the denominators to give

$$D(A_1) = \left(\frac{1 + \frac{2Cs^2}{\sigma^2} + \frac{2s^2}{\sigma^2}i}{\left(1 + \frac{2Cs^2}{\sigma^2}\right)^2 + \left(\frac{2s^2}{\sigma^2}\right)^2}\right)^{1/2} \exp\left(-T^2 \frac{(1+iC)(2\sigma^2 + 4Cs^2 + 4is^2)}{(2\sigma^2 + 4Cs^2)^2 + 16s^4}\right).$$

Finally, this can be simplified further to⁶

$$\begin{aligned} D(A_1) &= \sigma \left((\sigma^2 + 2Cs^2)^2 + 4s^4 \right)^{-1/4} \exp\left(\frac{1}{2}i \arctan\left(\frac{2s^2}{\sigma^2 + 2Cs^2}\right)\right) \\ &\quad \times \exp\left(-T^2 \frac{\sigma^2 \left[1 + i(C + (1+C^2)\frac{2s^2}{\sigma^2})\right]}{2[(\sigma^2 + 2Cs^2)^2 + 4s^4]}\right). \end{aligned}$$

⁶For $a, b \in \mathbb{R}$ $(a+bi)^{1/2} = (a^2+b^2)^{1/4} \exp\left(\frac{1}{2}i \arctan\left(\frac{b}{a}\right)\right)$.

From this expression it is clear that at equilibrium

$$\tilde{\sigma}^2 \sigma^2 = (\sigma^2 + 2Cs^2)^2 + 4s^4, \quad (3.16a)$$

$$\tilde{C} = C + (1 + C^2) \frac{2s^2}{\sigma^2}, \quad (3.16b)$$

$$\phi = \frac{1}{2} \arctan \left(\frac{2s^2}{\sigma^2 + 2Cs^2} \right), \quad (3.16c)$$

$$\zeta = \left(\frac{\sigma}{\tilde{\sigma}} \right)^{1/2}. \quad (3.16d)$$

The expressions for the chirp and variance can be verified by comparing to the dimensional equivalents from the literature [6, 7, 15, 17]. One finds

$$\left(\frac{T_1}{T_0} \right)^2 = \left(1 + \frac{C\beta_2 z}{T_0^2} \right)^2 + \left(\frac{\beta_2 z}{T_0^2} \right)^2, \quad \tilde{C} = C + (1 + C^2) \frac{\beta_2 z}{T_0^2},$$

with the conversions $T_0 = \sigma T_M$, $T_1 = \tilde{\sigma} T_M$, and $\beta_2 L_D T_0^{-2} = 2s^2 \sigma^{-2}$. In addition to this, the expression for ζ can be validated using conservation of energy. Within the **CFBG** energy is conserved, assuming everything is reflected, therefore,

$$\int_{-\infty}^{\infty} |A_1|^2 dT = \int_{-\infty}^{\infty} |A_2|^2 dT.$$

After substituting the expressions, this reduces to

$$h^2 P \int_{-\infty}^{\infty} e^{-T^2/\sigma^2} dT = h^2 P \zeta \int_{-\infty}^{\infty} e^{-T^2/\tilde{\sigma}^2} dT.$$

These expressions are easily integrated to show that $\sqrt{\pi\sigma^2} = \sqrt{\pi\tilde{\sigma}^2}\zeta^2$, and finally that

$$\zeta = \left(\frac{\sigma}{\tilde{\sigma}} \right)^{1/2}.$$

3.4.2 Equilibrium Shape of the Pulse

Now that the effect of dispersion is known analytically, the system (3.15) can be solved. The out-going variance and chirp can be eliminated from this system of equations using (3.15b) and (3.15c):

$$\tilde{\sigma}^2 = \frac{\sigma^2}{1 - \sigma^2}, \quad \tilde{C} = C \frac{1}{1 - \sigma^2}.$$

Combining this first expression with (3.16a) and expanding the square, we have

$$\frac{\sigma^4}{1 - \sigma^2} = \sigma^4 + 4C^2s^4 + 4Cs^2\sigma^2 + 4s^4,$$

or written as a polynomial in σ ,

$$0 = \sigma^6 + 4Cs^2\sigma^4 + (4s^4(C^2 + 1) - 4Cs^2)\sigma^2 - 4s^4(C^2 + 1). \quad (3.17)$$

The chirp can now be eliminated using (3.16b), the $1 + C^2$ can be reduced in order by noticing that

$$1 + C^2 = \frac{\sigma^4}{2s^2(1 - \sigma^2)} C.$$

Solving for C gives

$$C = \frac{\sigma^4}{2s^2(1 - \sigma^2)} \pm \sqrt{\frac{\sigma^8}{16s^4(1 - \sigma^2)^2} - 1} = \frac{\sigma^4 \pm \sqrt{\sigma^8 - 16s^4(1 - \sigma^2)^2}}{4s^2(1 - \sigma^2)}, \quad (3.18)$$

and after simplifying (3.17) algebraically, we arrive at

$$\frac{\sigma^6}{2 - \sigma^2} = \mp \sqrt{\sigma^8 - 16s^4(1 - \sigma^2)^2}. \quad (3.19)$$

As we shall see, σ is strictly less than 1 at equilibrium, and so, notice that the left hand side of this expression is strictly positive. Therefore, only the negative root of (3.18) will yield a solution. Moreover, Martinez, Fork, and Gordon [40] found two solutions to their discrete model (Section 2.3) analytically, but showed that one was unstable—consistent with experiments. After squaring each side of (3.19) we obtain the biquartic equation

$$(\sigma^2)^4 + 4s^4(\sigma^2)^3 - 20s^4(\sigma^2)^2 + 32s^4(\sigma^2) - 16s^4 = 0. \quad (3.20)$$

Since this is a quartic in σ^2 this can be solved analytically; the (positive, real) solution is

$$\sigma^2 = \sqrt{2}s \left(s^6 + 3s^2 + \sqrt{4 + s^4} (1 + s^4) \right)^{1/2} - s^4 - s^2 \sqrt{4 + s^4}. \quad (3.21)$$

A sample solution for the linear model is shown in Figure 3.2. To reiterate, the envelope at equilibrium is Gaussian, and therefore, so too is the Fourier transform. Also, the pulse is linearly chirped.

3.4.3 Asymptotic Expansion of the Variance

While (3.21) is useful, so too is the asymptotic behaviour. The asymptotic expansion provides additional information about the structure that the full analytic expression cannot. Moreover, the expansion provides more detail about the limits, as well has the rate of convergence. Lastly, the expansion allows for simplified expressions within their domains that are much less unwieldy than those found in the previous subsection.

We shall investigate the nature of the solution to (3.20) both when $s \rightarrow 0$ (a very short CFBG), as well as when $s \rightarrow \infty$ (a very long CFBG). For ease of notation,

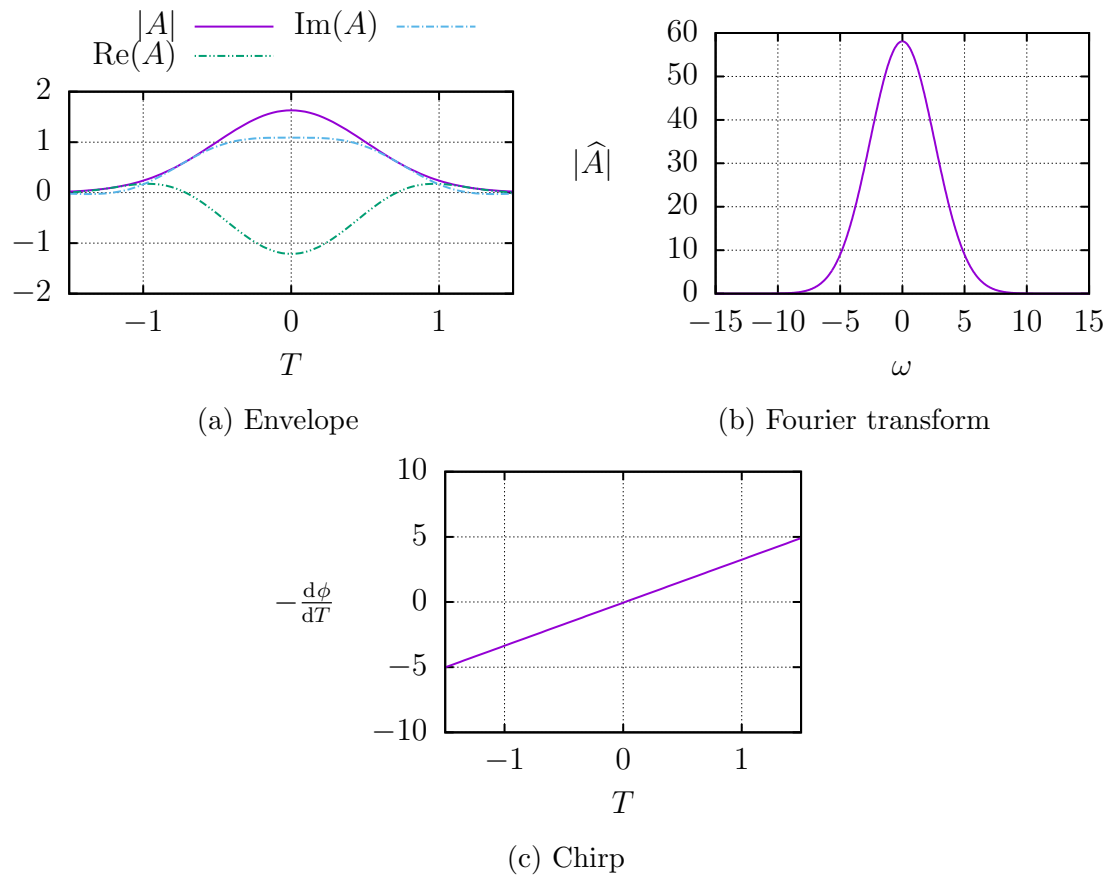


Figure 3.2: Equilibrium state of the pulse for the parameters $s = 0.15$ (dispersion), $b = 0$ (nonlinearity), $a = 8000$ (gain), and $h = 0.04$ (loss) as defined by (3.18) and (3.21).

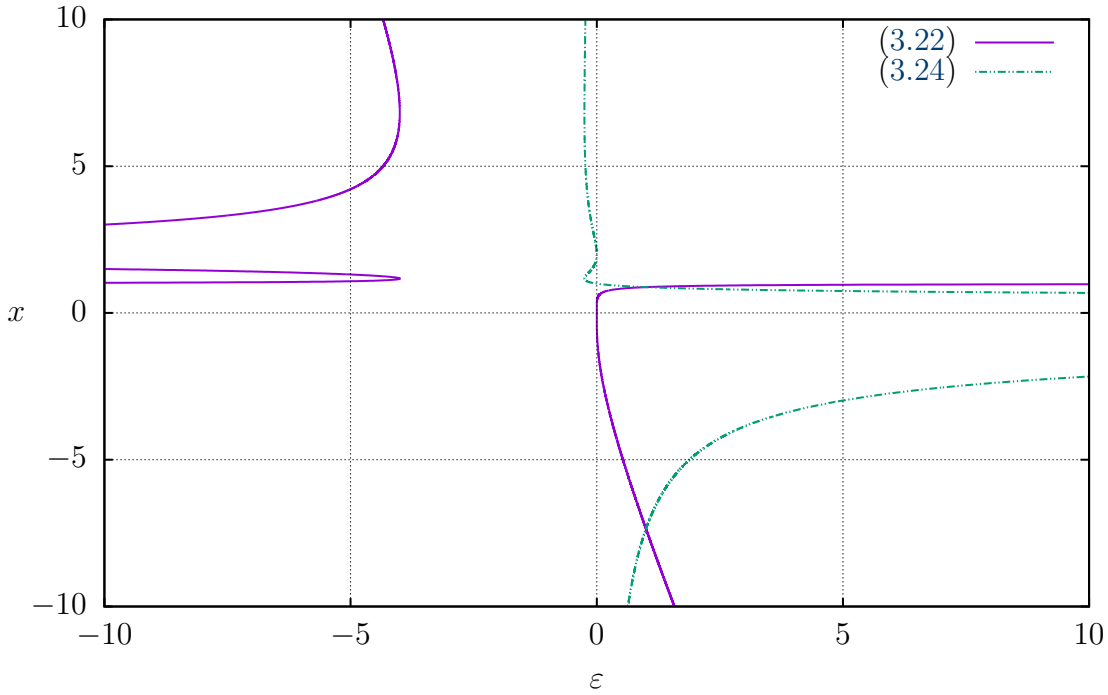


Figure 3.3: Plot of (3.22) and (3.24) to highlight the structure.

(3.20) is rewritten as

$$\frac{1}{4}x^4 = -\varepsilon(x-1)(x-2)^2, \quad (3.22)$$

where $x = \sigma^2$, $\varepsilon = s^4$, and $\varepsilon \rightarrow 0$. Figure 3.3 shows (3.22) graphically. Additionally, suppose x can be expanded as a power series in ε :

$$x = x_0 + x_1\varepsilon^\alpha + x_2\varepsilon^\beta + \dots \quad (3.23)$$

with $0 < \alpha < \beta$. Then, expanding (3.22) using (3.23) and collecting terms, at $\mathcal{O}(1)$,

$$\frac{1}{4}x_0^4 = 0,$$

and so, $x_0 = 0$. Knowing this, we consider how to balance

$$\frac{1}{4}x_1^4\varepsilon^{4\alpha} = \varepsilon(-x_1^3\varepsilon^{3\alpha} + 5x_1^2\varepsilon^{2\alpha} - 8x_1\varepsilon^\alpha + 4).$$

In order to have dominant balance it must be that the left hand side balances with the final term of the right hand side, that is, $4\alpha = 1$, or $\alpha = \frac{1}{4}$. Therefore, at $\mathcal{O}(\varepsilon)$ $x_1^4 = 16$, or

$$(x_1 - 2)(x_1 + 2)(x_1^2 + 4) = 0,$$

and so, $x_1 = \pm 2, \pm 2i$. However, we require x to be positive and real—recall that $x = \sigma^2$ —thus, we take $x_1 = 2$. Now, the next lowest order of the left hand side must be $\varepsilon^{3\alpha+\beta} = \varepsilon^{3/4+\beta}$. As with the previous iteration, this must balance with the lowest order term of the $8x$. Hence, $\frac{3}{4} + \beta = 1 + \alpha = \frac{5}{4}$, thus, $\beta = \frac{1}{2}$. Now, at $\mathcal{O}(\varepsilon^{5/4})$,

$$\frac{1}{4}4x_1^3x_2 = -8x_1,$$

and with the choice of $x_1, x_2 = 2$. Combining these results gives $x = 2\varepsilon^{1/4} - 2\varepsilon^{1/2} + \mathcal{O}(\varepsilon^{3/4})$, or $\sigma^2 = 2s(1-s) + \mathcal{O}(s^3)$, this is shown in Figure 3.4. The choice $\varepsilon = s^4$ was for convenience, but in retrospect, $\varepsilon = s$ yields a cleaner, but identical, solution.

We shall now consider the other limit, when the dispersion parameter, s , approaches ∞ . Using a similar substitution we instead write (3.20) as

$$\frac{1}{4}\varepsilon x^4 = -x^3 + 5x^2 - 8x + 4, \tag{3.24}$$

where $x = \sigma^2$, and $\varepsilon = s^{-4}$ instead so we still have $\varepsilon \rightarrow 0$, this is also shown in

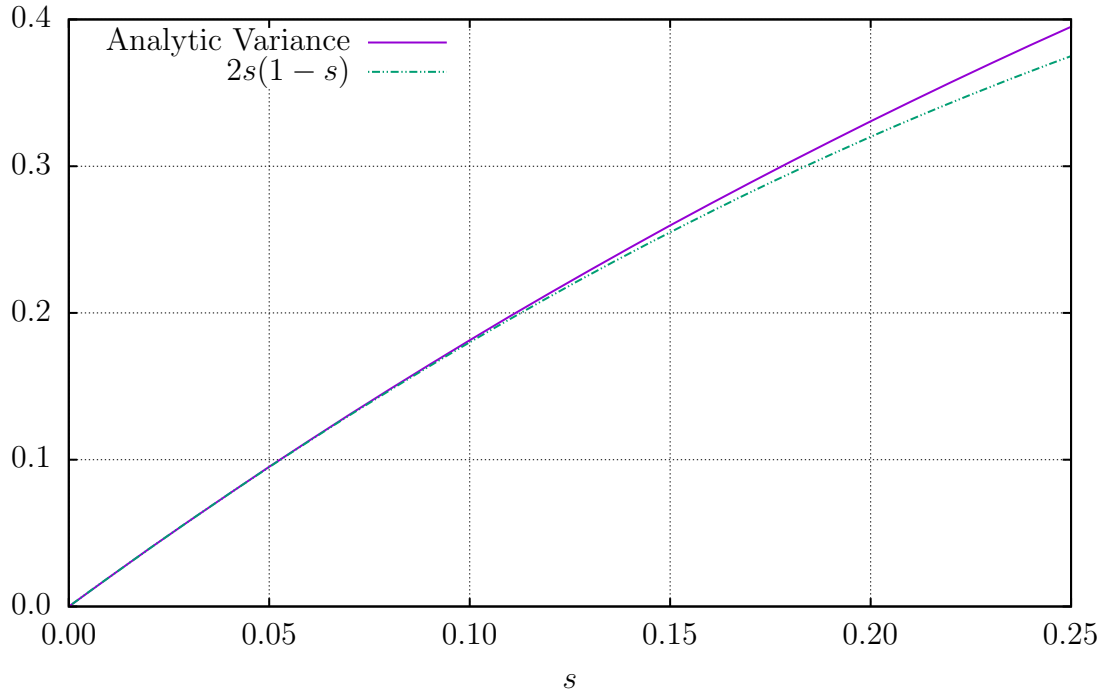


Figure 3.4: Asymptotic expansion of the variance as the dispersion parameter, s , approaches 0.

Figure 3.3. Furthermore, we must make a correction to the series expansion:

$$x = \varepsilon^{-\xi} (x_0 + x_1 \varepsilon^\alpha + x_2 \varepsilon^\beta + \dots). \quad (3.25)$$

The reason for this is because (3.24) is now singular—when $\varepsilon = 0$ the equation transforms from a quartic to a cubic, losing a root. As with before, we obtain dominant balance when the quartic term balances with the cubic term which occurs when $1 - 4\xi = -3\xi$, or $\xi = 1$. Then to $\mathcal{O}(\varepsilon^{-3})$, expression (3.24) gives

$$x_0^3(x_0 + 4) = 0.$$

The non-trivial solution $x_0 = -4$ gives rise to a boundary layer structure. However, this is unphysical because $x \geq 0$, leaving $x_0^3 = 0$, so this singular perturbation does not generate the boundary layer expected. Therefore, (3.25) reduces to a regular

perturbation problem, and α must equal 1. The next condition occurs at $\mathcal{O}(1)$ where

$$0 = -x_1^3 + 5x_1^2 - 8x_1 + 4 = -(x_1 - 1)(x_1 - 2)^2,$$

so either $x_1 = 1$ or $x_1 = 2$. The following term obtains dominant balance when the left hand side balances with the linear term of the right hand side, that is, when $\beta = 2$ provided⁷ $x_1 \neq 2$. Now at $\mathcal{O}(\varepsilon)$,

$$\frac{1}{4}x_1^4 = -3x_1^2x_2 + 5 \cdot 2x_1x_2 - 8x_2 = -x_2(3x_1 - 4)(x_1 - 2),$$

where the coefficients come from the binomial expansions. From this it is clear that

$$x_2 = \frac{-x_1^4}{4(3x_1 - 4)(x_1 - 2)}.$$

Thus, $x_1 = 1$, $x_2 = -\frac{1}{4}$, and

$$x = 1 - \frac{1}{4}\varepsilon + x_2\varepsilon^{\gamma-1} + \dots$$

Expanding one final term we find $\gamma = 3$, and to $\mathcal{O}(\varepsilon^2)$,

$$\frac{1}{4}4x_2x_1^3 = -(3x_3x_1^2 + 3x_2^2x_1) + 5(2x_3x_1 + x_2^2) - 8x_3.$$

Knowing the values of x_1 and x_2 this is simply an arithmetical calculation yielding $x_3 = \frac{3}{8}$. Finally,

$$x = 1 - \frac{1}{4}\varepsilon + \frac{3}{8}\varepsilon^2 + \mathcal{O}(\varepsilon^3),$$

⁷In the case of $x_1 = 2$ we find $\beta = \frac{3}{2}$ which leads to complex roots.

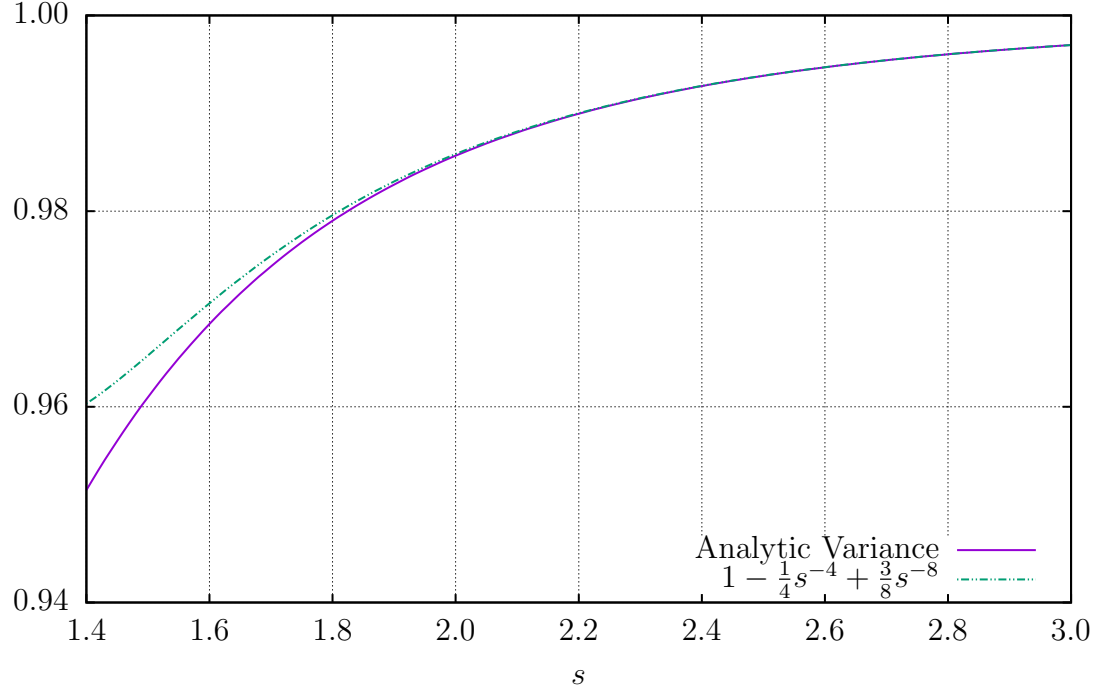


Figure 3.5: Asymptotic expansion of the variance as the dispersion parameter, s , approaches ∞ .

or,

$$\sigma^2 = 1 - \frac{1}{4s^4} + \frac{3}{8s^8} + \mathcal{O}(s^{-12})$$

this approximation is shown in Figure 3.5.

In conclusion, the asymptotic expansions of the observables are

$$\begin{aligned} \sigma^2 &= \begin{cases} 2s(1-s) + \mathcal{O}(s^3) & s \rightarrow 0 \\ 1 - \frac{1}{4s^4} + \frac{3}{8s^8} + \mathcal{O}(s^{-12}) & s \rightarrow \infty \end{cases} & C &= \begin{cases} 1 - s + \frac{1}{2}s^2 + \mathcal{O}(s^3) & s \rightarrow 0 \\ \frac{1}{2s^2} - \frac{3}{8s^6} + \mathcal{O}(s^{-10}) & s \rightarrow \infty \end{cases} \\ \frac{C}{\sigma^2} &= \begin{cases} \frac{1}{2s} - \frac{1}{8}s + \mathcal{O}(s^3) & s \rightarrow 0 \\ \frac{1}{2s^2} - \frac{1}{4s^6} + \mathcal{O}(s^{-10}) & s \rightarrow \infty \end{cases} & \zeta &= \begin{cases} 1 - \frac{1}{2}s + \frac{1}{8}s^2 + \mathcal{O}(s^3) & s \rightarrow 0 \\ \frac{1}{4^{1/4}s} - \frac{3 \cdot 4^{3/4}}{32s^5} + \mathcal{O}(s^{-9}) & s \rightarrow \infty. \end{cases} \end{aligned} \quad (3.26)$$

The general form of these is as expected. When $s \rightarrow 0$, we effectively remove the

CFBG from the cavity. This causes the pulse to be perpetually modulated, and so, the pulse's shape approaches a δ function, and therefore, $\sigma^2 \rightarrow 0$. Moreover, since ζ is the ratio of the amplitude of the pulse before and after dispersion, $\zeta \rightarrow 1$. In the opposite extreme, $s \rightarrow \infty$, the length / strength of the **CFBG** approaches infinity—this causes the pulse to broaden greatly, while conserving its energy. Because of this, the variance approaches unity because the shape is entirely determined by the modulation function. Additionally, $\zeta \rightarrow 0$ because the pulse becomes infinitely wide, and thus, the amplitude becomes infinitesimally small. Due to the expansive nature, the chirp approaches zero because any chirp will be expanded away.

3.4.4 Equilibrium Energy

Up until this point the \sqrt{P} factor has remained undetermined, however, it can be found once the equilibrium energy is known. From (3.15a) the equilibrium energy can be found, as well as the equilibrium peak power. This relation can be simplified by squaring both sides and rearranging to give

$$\frac{1}{h^2\zeta^2}E = W(aEe^E),$$

where, once again, W is the Lambert W function. Then, by taking the exponential of each side, and multiplying by this expression, we obtain⁸

$$\frac{1}{h^2\zeta^2}E \exp\left(\frac{1}{h^2\zeta^2}E\right) = W(aEe^E) \exp(W(aEe^E)) = aEe^E.$$

⁸By (A.1).

Now, this can be written as

$$\begin{aligned} ah^2\zeta^2 &= \exp\left(\frac{1}{h^2\zeta^2}E - E\right), \\ \log(ah^2\zeta^2) &= E\left(\frac{1}{h^2\zeta^2} - 1\right). \end{aligned}$$

The energy of the pulse entering the gain fibre at equilibrium is thus

$$E = \frac{h^2\zeta^2}{1 - h^2\zeta^2} \log(ah^2\zeta^2).$$

This expression allows us to determine a restriction on the parameters for a solution of the form (3.11) to exist—in order for this energy to be positive, $ah^2\zeta^2 > 1$. The energy of the pulses as it enters the optical coupler can now be found, recall from (3.1) that the energy is defined as

$$E = \int_{-\infty}^{\infty} |A|^2 dT;$$

the energy entering the optical coupler is then

$$E_* = \int_{-\infty}^{\infty} |G(A)|^2 dT = \frac{W(aEe^E)}{E} \int_{-\infty}^{\infty} |A|^2 dT = W(aEe^E). \quad (3.27)$$

We can now find the amplitude of the pulse as well now that the energy is known—as we have previously found the equilibrium shape. Again, from (3.1), it must be that $E_* = \sqrt{\pi}P\sigma$, or,

$$P = \frac{W(aEe^E)}{\sqrt{\pi}\sigma}. \quad (3.28)$$

The asymptotic expansions when $s \rightarrow 0$ of the energy, and peak power are—for

completeness—

$$E_* = \Lambda - \Theta \frac{\Lambda}{1 + \Lambda} s + \mathcal{O}(s^2), \quad P = \frac{\Lambda}{\sqrt{2\pi}s} + \left(\frac{\Lambda}{2} - \Theta \frac{\Lambda}{1 + \Lambda} \right) \sqrt{\frac{s}{2\pi}} + \mathcal{O}(s^{3/2}), \quad (3.29)$$

respectively, where

$$\Lambda = W\left(\frac{ah^2 \ln(ah^2)}{1 - h^2} \exp\left(\frac{h^2 \ln(ah^2)}{1 - h^2}\right)\right),$$

and

$$\Theta = \frac{(h^2 \ln(ah^2) + 1 - h^2)(\ln(ah^2) + 1 - h^2)}{(1 - h^2)^2 \ln(ah^2)}.$$

3.5 Chapter Summary

In this chapter we first derived the effect each of the five components—gain, nonlinearity, loss, dispersion, and modulation—has on the incoming pulse from (2.4). Furthermore, to highlight the structure of these effects the system was non-dimensionalized. This yielded the functional maps (3.8) for the components, with corresponding non-dimensional parameters (3.9). With all of the operators defined, we proceeded to compose each process, in the order most representative of a tuneable laser, to give the effect of one complete circuit around the laser cavity.

We then sought a solution to the linearized model—having omitted the nonlinearity component. In this case, we were able to find a closed form analytic solution for the equilibrium state. To do this, we assumed the solution took the form of a linearly chirped Gaussian, (3.11), which was then passed through each process map yielding (3.14) in the end. The fixed point of the linearized model was found by

equating (3.11) and (3.14), but, allowing a phase shift to have occurred. The equilibrium variance, chirp, energy, and peak power were found to be (3.21), (3.18), (3.27), and (3.28), respectively. To gain a better understanding of the limiting behaviour, the asymptotic expansions were investigated. This yielded (3.26) for the asymptotic expansions of the variance and chirp, and (3.29) for the energy and peak power.

With the linear model fully solved, we shall now turn our attention to the rich structure added by the full nonlinear model.

Chapter 4

Solution of the Nonlinear Model

We shall now consider the nonlinear case—when $b > 0$. In this case it becomes impossible to obtain an analytic result. Recall from (3.8b) that the nonlinearity takes the form

$$F(A) = A e^{ib|A|^2}.$$

This is a highly nonlinear operator, and attempting to compute the Fourier transform analytically of a pulse that has undergone the transformation due to the nonlinearity is futile. Instead we must resort to a numerical solution.

4.1 Code

Finding the solution numerically will be done in a similar manner as with the analytic linear solution. Using Python, a function is written for each component of the laser cavity given by (3.8); an initial pulse is iteratively passed from function to function in the hopes that a fixed point is found. The full Python code can be found in Appendix C.

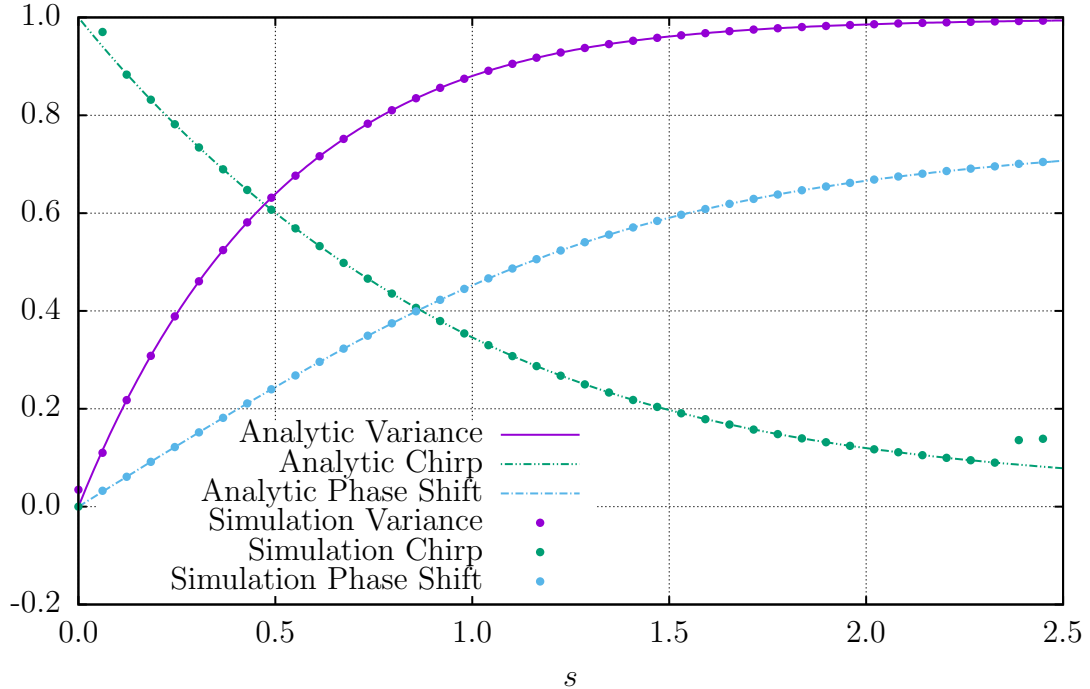


Figure 4.1: Simulation and analytic equilibrium variance, chirp, and phase shift as a function of the dispersion parameter, s . The analytic expressions are given by (3.21), (3.18), (3.16c), respectively.

4.1.1 Validation

Before delving into the nonlinear behaviour of the model, we wish to validate that the code is working as expected by comparing the results of the simulations with $b = 0$ to the results of the linear model in Chapter 3. In the case of the numerical solution, our initial conditions become somewhat important for two reasons. First, if the energy is too high initially the nonlinear effects will be too strong leading to **self-phase modulation**. Secondly, the initial waveform needs to be well behaved enough so that the Fourier transform is band limited. In all of the following analysis the initial waveform is $\Gamma \operatorname{sech}(2T)e^{i\pi/4}$ normalized so that the initial energy is $E_0 = 0.1$; additionally, $a = 8000$, and $h = 0.04$.

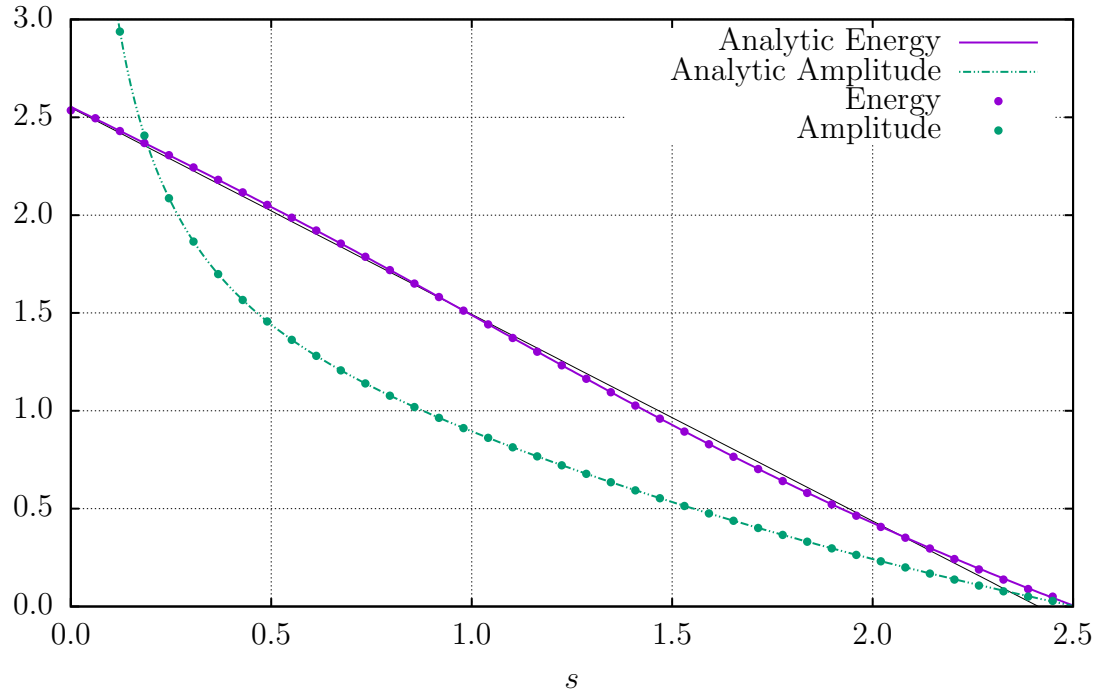


Figure 4.2: Equilibrium energy, and peak power of the pulse as a function of the dispersion parameter, s . The thin black line is the line of best fit to highlight that the energy is *not* linearly dependent on s .

In the first experiment the pulse is allowed to equilibrate for 40 loops of the circuit¹, we then compare the variance, chirp, and phase shift of the analytic and numerical solutions. The results of this are shown in Figure 4.1. For the most part, we see exceptional agreement between the analytic solution and numerical solution for the variance, and phase shift. However, as $s \rightarrow 2.5$ the chirp from the simulations begins to deviate from the analytic solution. The reason for this is quite a simple one. We shall turn our attention to the energy, and amplitude of the pulse at equilibrium as shown in Figure 4.2. As with Figure 4.1, there is very good agreement between the two solutions. It is also now clear that at approximately $s = 2.5$ there is too much dispersion—the pulse is no longer sustainable. This is of course a consequence of the condition (3.15a). Since the pulse effectively vanishes after this point, the chirp calculation becomes numerically unstable leading to the disagreement.

¹The choice of 40 will be justified in the following section.

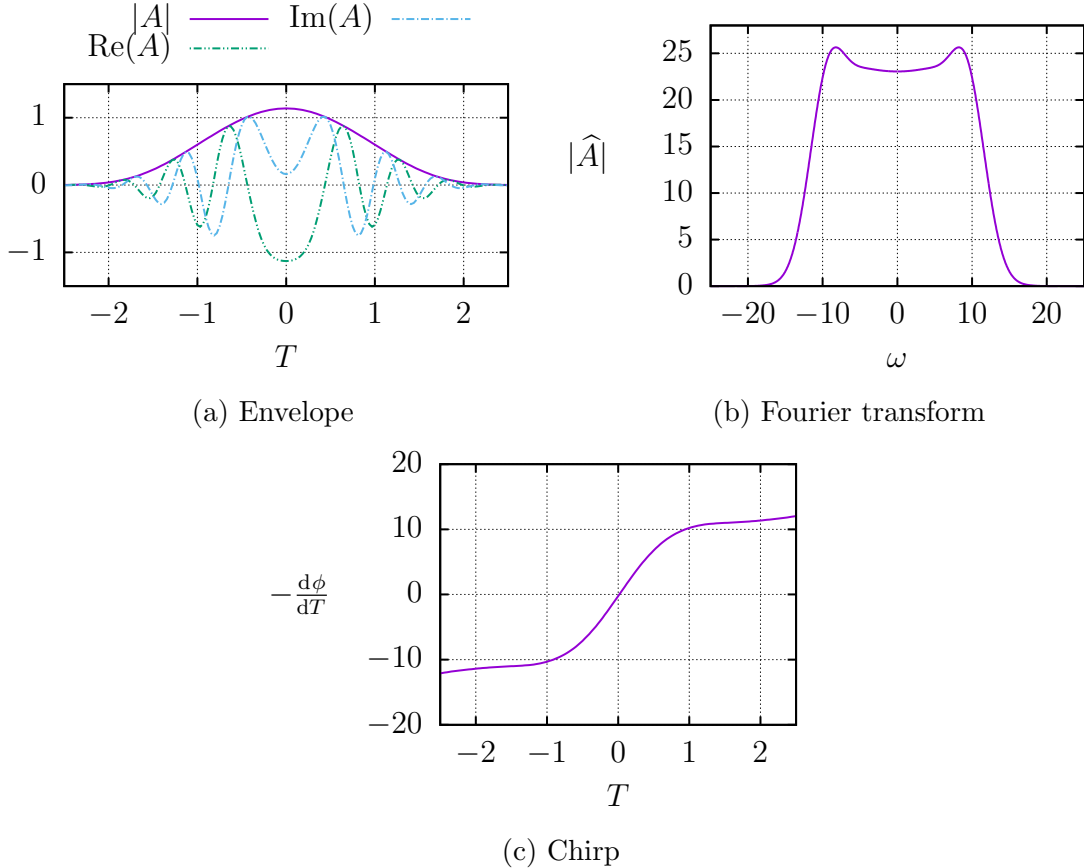


Figure 4.3: Simulation with $s = 0.15$, and $b = 2.1$ after 15 circuits.

With the numerical solution yielding the expected results we are now ready to explore the rich structure that the nonlinearity adds.

4.2 Nonlinear Model

With the inclusion of the nonlinearity we generally find a similar solution to the linear case. An example of this is shown in Figure 4.3. The envelope of the pulse is unsurprisingly Gaussian-esque, however, it is *not* precisely Gaussian and more closely resembles a generalized Gaussian². The fact that the pulse envelope is not Gaussian is further emphasized while examining the Fourier transform of the pulse. If the pulse

²A generalized Gaussian has the form $\exp(-t^\alpha)$, with $\alpha > 2$.

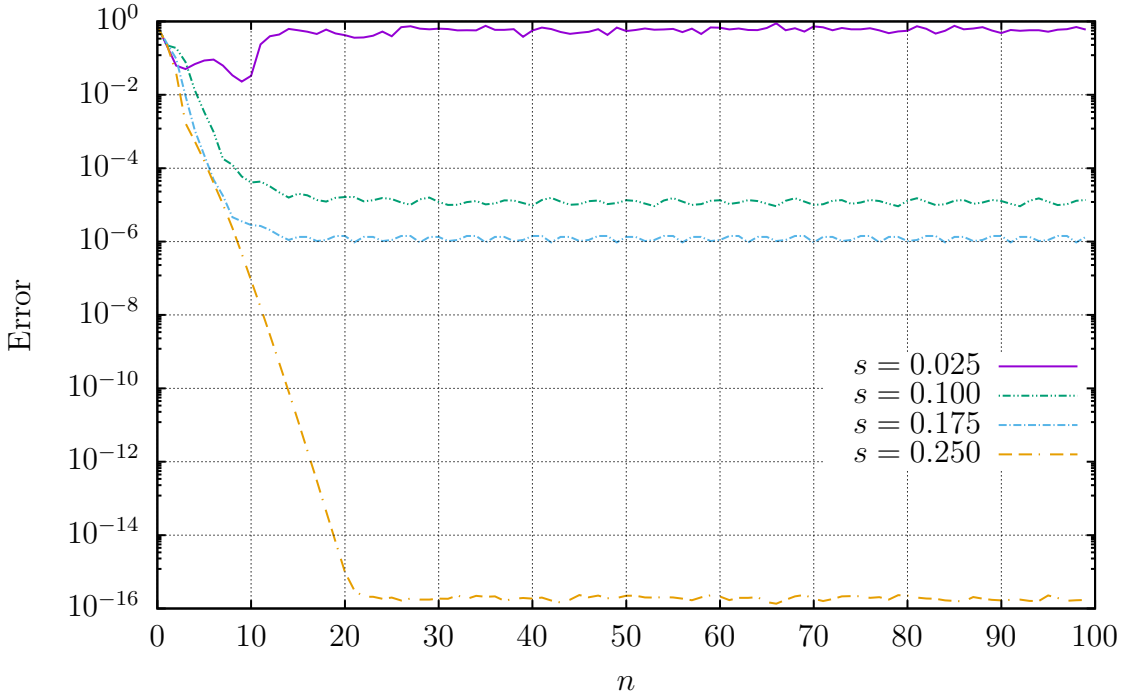


Figure 4.4: Rate of convergence as a function of number of iterations for various s values, with $b = 0.5$. The error is given by (4.1).

were a Gaussian, we would expect the Fourier transform to also be a Gaussian [43, 44]. Instead, the magnitude of the Fourier transform has a unique weakly bi-modal shape. This deviation suggests the nonlinearity implants higher frequency oscillations into the pulse—a key observation in the coming subsections. Finally, we shall examine the derivative of the phase—essentially the chirp. Recall in Chapter 3 the chirp was defined as coefficient of $-\frac{1}{2}iT^2$ in the exponential, and by taking the negative of the derivative we would expect a linear function with a slope equal to the chirp. In the nonlinear case, we recover this linear response for moderate values of T . However, for $|T| > 1$ the chirp begins to saturate. This is consistent with the experimental results [21, 46, 49].

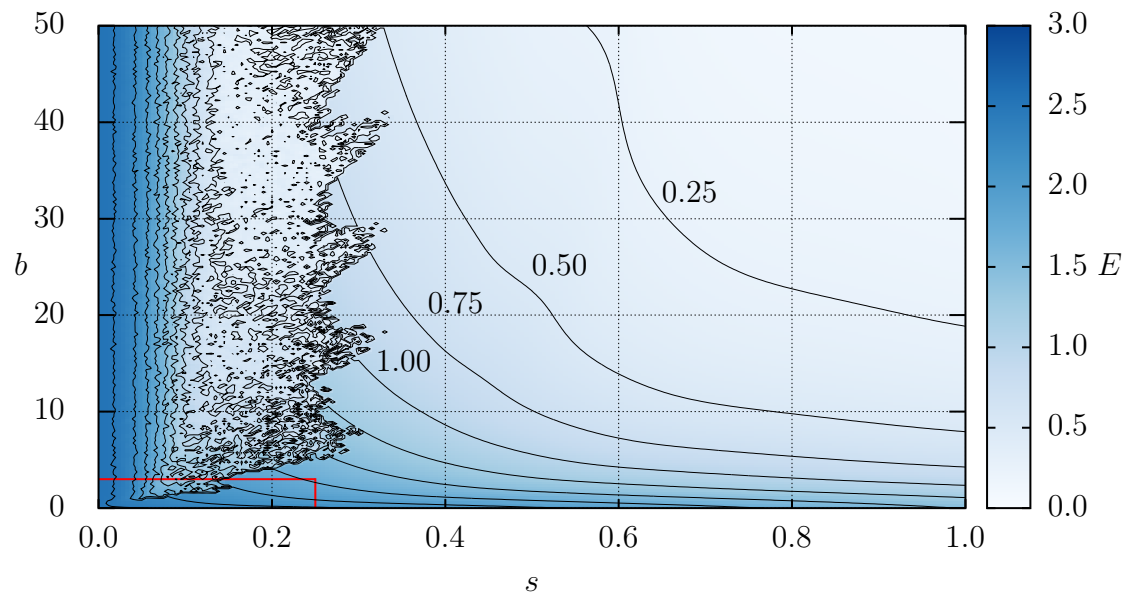
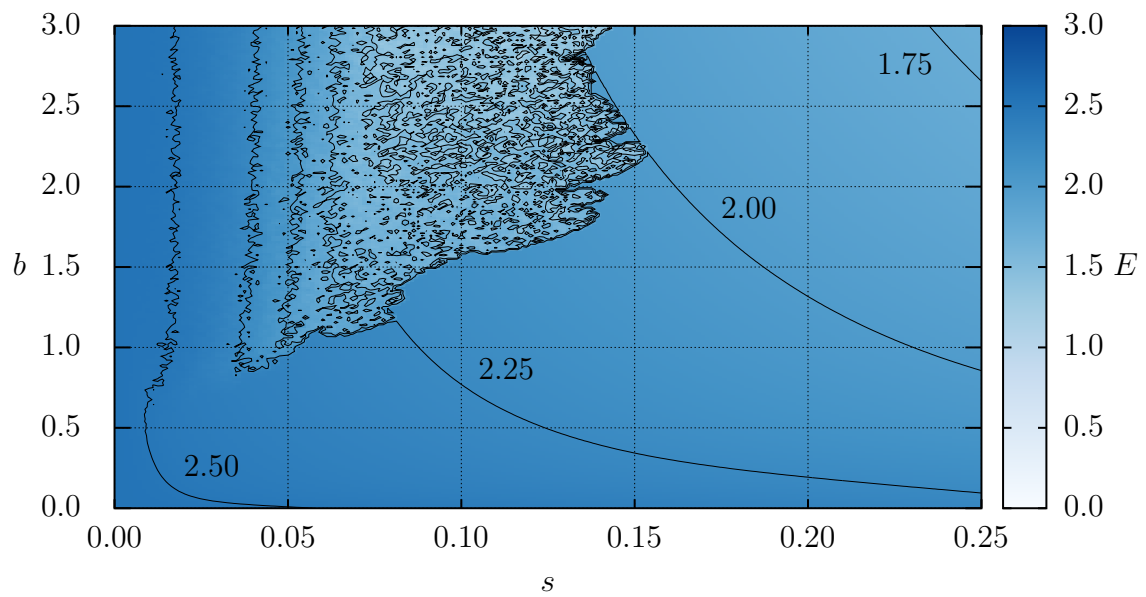
(a) Energy of the pulse within the s - b plane.(b) Regime corresponding to typical s , and b values for tuneable lasers.

Figure 4.5: Energy of the pulse after 100 cycles. The energy is constant along the black lines.

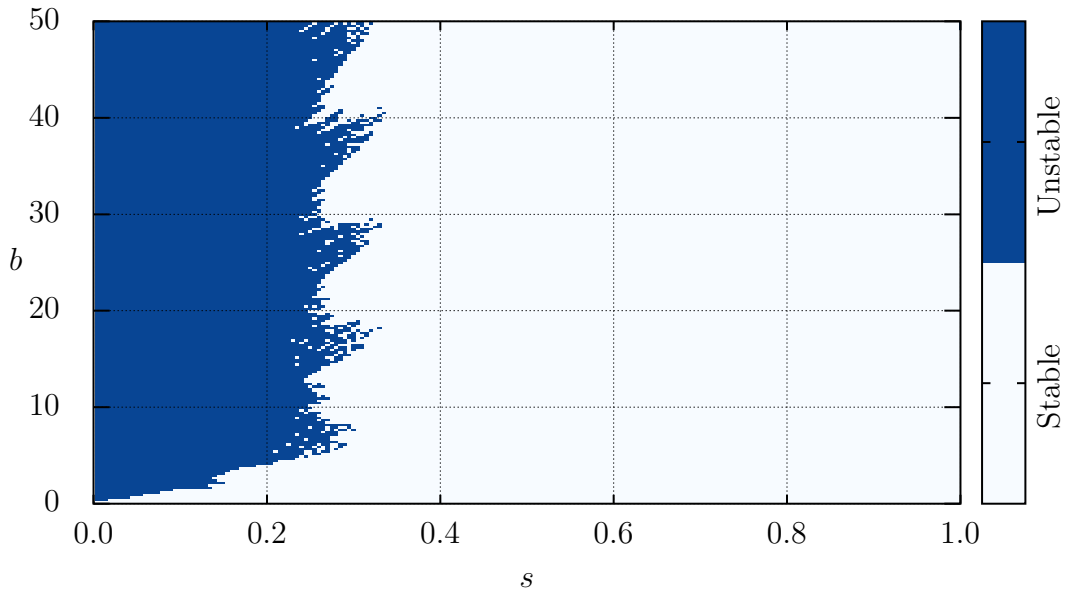


Figure 4.6: Stability of the pulse in the s - b plane.

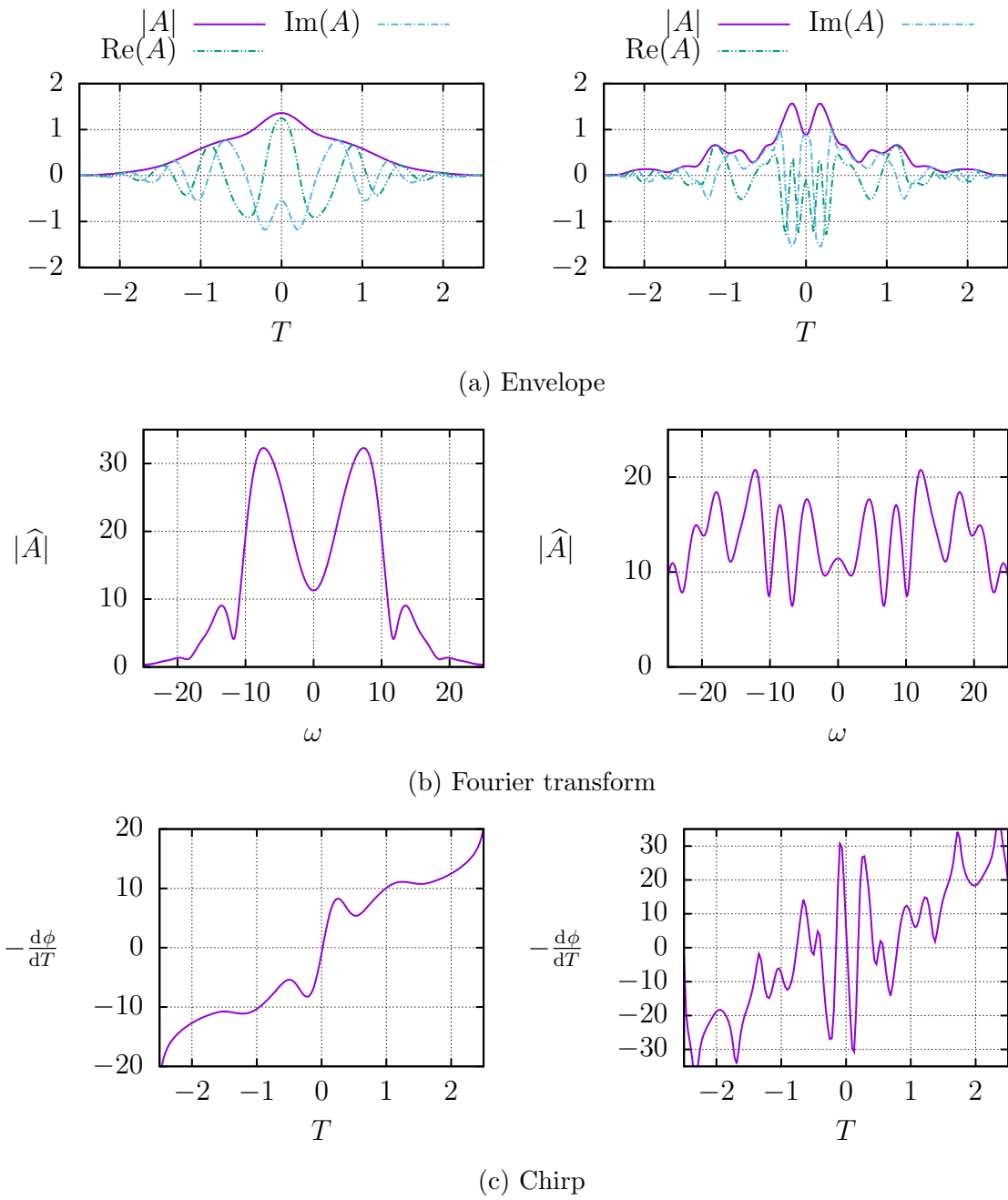
4.2.1 Energy

The energy of the pulse is directly related to the output power of the laser, and since this is not as controllable as in a regular laser, it is of great interest. In this nonlinear case we allow the initial pulse to pass through each component 100 times instead of 40 in the linearized case. This choice can be justified by Figure 4.4. The pulse reaches a state in which the error no longer decreases within typically 10–20 iterations. In the linearized case we chose to iterate 40 times since this is about double the number of iterations expected. Furthermore, in the nonlinear case we extend this number further to 100 in case the nonlinearity increases the number of iterations required to converge. The energy of the pulse after 100 iterations is shown in Figure 4.5. In Figure 4.5b we generally find that the energy is a smooth surface that slowly decays as s and b increase. In the upper left hand region of the plot this is clearly not the case. The contours show that the energy is very noisy with very large derivatives.

Perhaps more surprising, as shown in Figure 4.5a, is that this boundary between periodic and aperiodic behaviour appears to become periodic (in the parameter space) as b increases around $s = 0.3$. These features are further highlighted in Figure 4.6 by disregarding the energy and only examining whether the pulse is invariant after additional iterations.

Self-Phase Modulation and Wave Breaking

The noise in the energy exhibited for moderate to large values of b , and small values of s is a phenomenon called *wave breaking* [15, 17, 20, 21, 46]. Wave breaking is not limited to just optics; wave breaking occurs in areas such as plasmas, transmission lines, and fluid dynamics [21]. Wave breaking occurs because the pulse begins to interfere with itself in a way called self-phase modulation (SPM) [8, 10, 15]. SPM occurs because the index of refraction is intensity dependent [6, 8, 10, 21], which leads to additional chirp across the pulse [6, 15, 17, 21]. This in turn causes higher order frequencies to be injected into the pulse [15, 17], as we saw in Figure 4.3. These high frequencies compound with each trip around the cavity becoming parasitic very quickly—Figure 4.7 highlights this. Notice that the difference between Figure 4.3 and Figure 4.7 is a difference in b of 0.05—just enough to cross the boundary—this difference could be attributed to adding a few centimetres more of fibre between the gain and output coupler. The left figures show the pulse after 11 trips around the cavity; in the Fourier transform it is clear that the contributions from higher frequencies has increased. We obtain comparable results as in the experiments [17, 21]. Additionally, the chirp starts losing its linearity causing it to start becoming unstable; the nature of this instability is again in agreement with the experiments [17, 21]. The parasitic nature of the high frequency contributions is evident by examining the right figures. After five additional trips around the cavity, the envelope of the pulse is much more

Figure 4.7: $s = 0.15$, $b = 2.15$, **Left:** 11 loops, **Right:** 16 loops

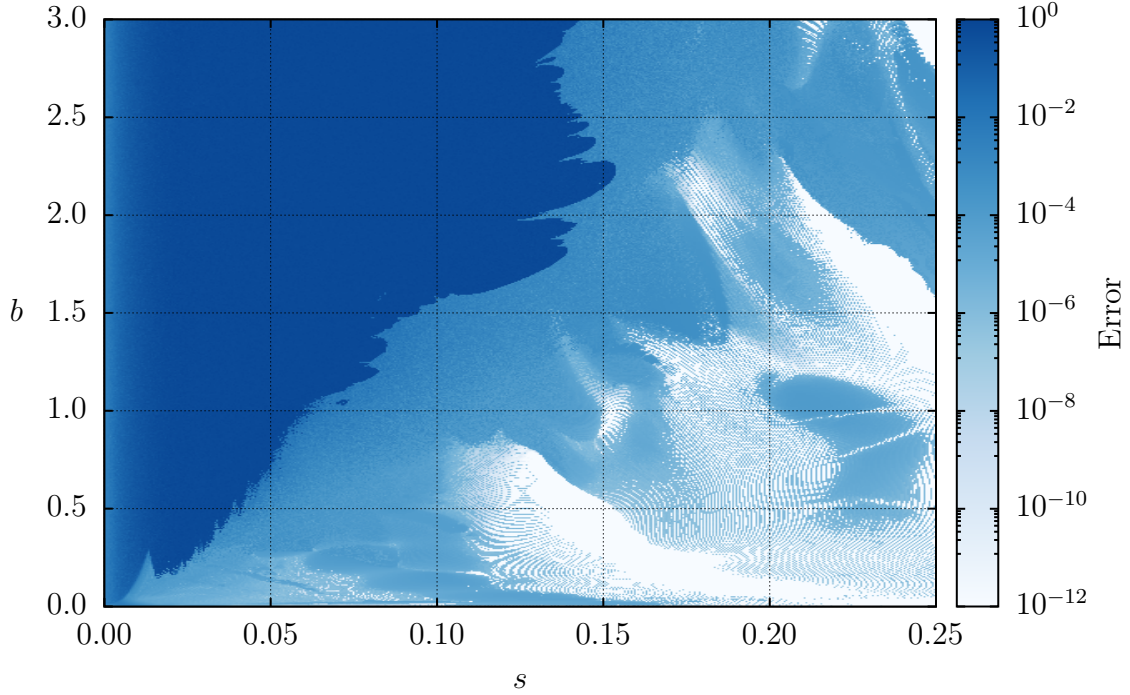


Figure 4.8: Error of the pulse (given by (4.1)) between iterations 99 and 100.

rippled, and the real and imaginary parts become incoherent. Moreover, the Fourier transform has no clear structure and has essentially become noise. The chirp has grown to be highly oscillatory and unstable. Once the pulse has reached a state such as this, the envelope, Fourier transform, and chirp never reach a steady equilibrium state.

4.2.2 Convergence

To obtain a better understanding of how the pulse either converges to equilibrium, or diverges to wave breaking, we shall examine the difference between the envelopes of consecutive iterations. More precisely, we compute the error by

$$E = \frac{\| |A_i| - |A_{i-1}| \|_2}{\| |A_{i-1}| \|_2}, \quad (4.1)$$

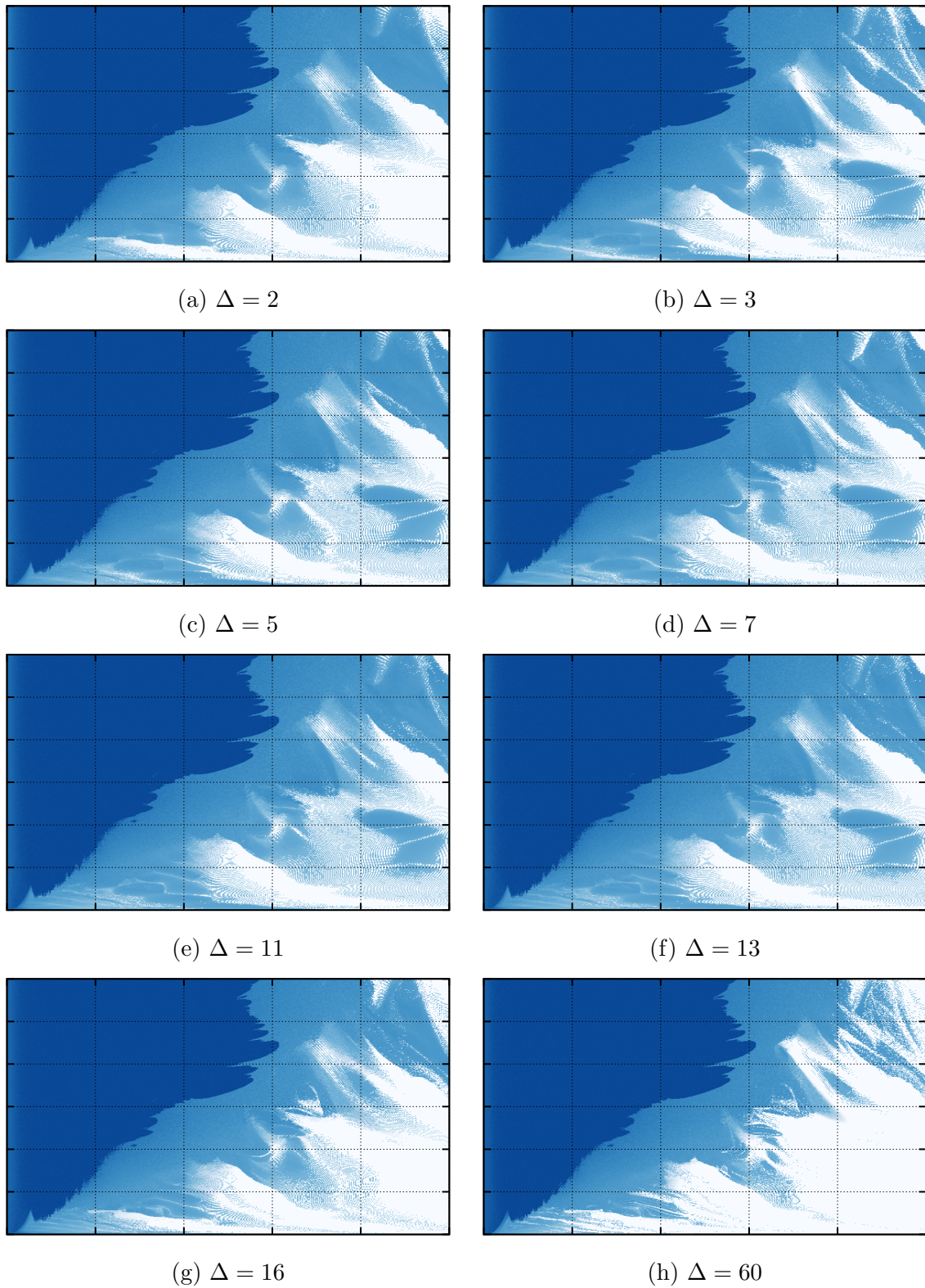


Figure 4.9: Error for various values of Δ , the colour bar and axis labels have been omitted for clarity, the scales and ranges are the same as in Figure 4.8.

where $\|\cdot\|_2$ denotes the $L^2(\mathbb{R})$ norm, which is computed numerically using the trapezoid rule ($N = 2^{12}$). Notice as well that in the numerator we use the modulus of the pulses, again this is because we are uninterested in the phase shift between iterations. A plot of the error can be found in Figure 4.8, with $i = 100$. The standard method would be to iterate until a fixed tolerance is reached, however, there are some reasons that make a fixed number of iterations preferable—as long as a sufficient number is chosen. The main reason is that this allows us to observe a richer structure than simply whether or not the tolerance had been reached by some maximum number of iterations. Additionally, incorrectly choosing the critical tolerance could easily lead to erroneous categorizations at points. As we saw in Figure 4.4 some values of the parameters lead to a steady, periodic state, but with an error of $\mathcal{O}(10^{-6})$, and so, had we set the tolerance to 10^{-8} these points would have been labeled as unsteady.

Unsurprisingly, the error is largest in the region where the wave breaks. As mentioned in the previous subsection, the pulse does not reach a stable state in this region. As a consequence the envelope varies drastically, which leads to this large error. Conversely, the region where the energy appeared to be stable still has a non-zero error. The cause of this discrepancy is because some equilibrium states have a periodicity greater than 1, thus, we redefine (4.1) to be instead

$$E_\Delta = \frac{\||A_i| - |A_{i-\Delta}|\|_2}{\|A_{i-\Delta}\|_2}, \quad (4.2)$$

to pick up equilibrium states with period Δ , again with $i = 100$. Figure 4.9 shows the error for an assortment of Δ values. There are several key observations to make, first, for $\Delta = 2$ the kidney-shaped blob in the lower right corner has vanished, thus, this entire region has a periodicity of 2. Second, for $\Delta = 3$ in the upper right corner a negative triangular-shaped structure emerges. Lastly, $\Delta \in \{5, 7, 11, 13\}$ may not

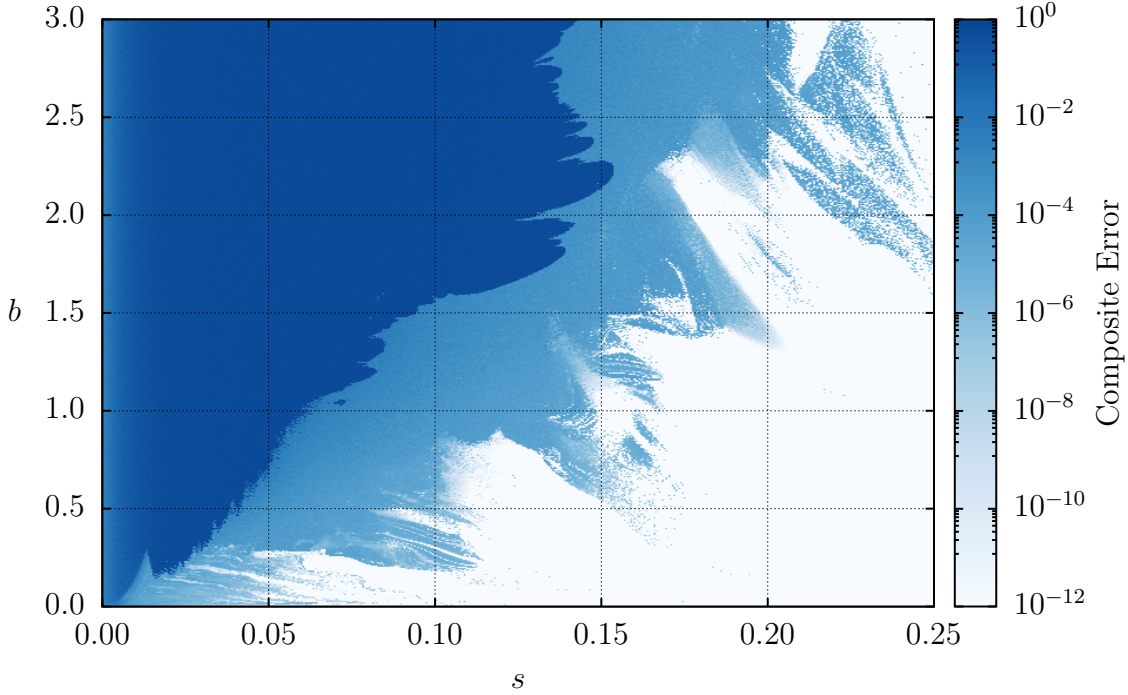


Figure 4.10: Composite error, (4.3), of Figure 4.9.

seem to extract any higher order periods, however, there are in fact very small striations in the lower left. We typically chose Δ values to be prime since they are the building blocks for composite numbers. However, there are two composite Δ values of interest. The first is 16, since $16 = 2^4$, as it will pick up any periodic behaviour with orders of 2, 4, 8, 16. Lastly, we chose $\Delta = 60$ for a similar reason: because 60 is highly divisible we can extract orders such as 12 or 30 without having to explicitly run the calculations³.

We now have the data to make a more meaningful estimate of the error between iterations. To compute this composite error we take the minimum of the error from each of these calculations:

$$E_c = \min_{\Delta} \{E_{\Delta}\}. \quad (4.3)$$

³In the case of $\Delta = 60$ a value of $i = 150$ is used to ensure sufficient iterations to converge.

The intriguing structure of the composite error is shown in Figure 4.10. Compared with the error from Figure 4.8 the lower right region is much more well behaved, that is, the error is a few orders of magnitude lower. A peculiar trait of the band between the unstable and stable regions is that within this area the pulse is in a quasi-stable state—the pulse is stable and has reached a sort of equilibrium, however, the envelope of the pulse has small variations with no clear period. Additionally, there appears to be no periodicity of the envelope within the wave breaking region, further supporting the claim that the pulse here is completely unstable.

4.2.3 Permutation of Components

The last item we wish to consider is the order in which the components are placed. In Section 3.3 a brief description for the choice of the order was given. We start with the loss component since this coincides with the output; the fibre nonlinearity follows the gain since this is where it has the largest impact; and the loss follows the nonlinearity in an attempt to mitigate its effect. Therefore, the loss is first, and the gain followed by the nonlinearity are last—leaving dispersion and modulation in the middle. We chose to put the dispersion block ahead of the modulator. However, there was no real reason behind this—modulation before dispersion is equally as valid—and in this subsection we explore the effect of modulating the pulse before it passes through the CFBG.

The result of this switch is shown in Figure 4.11. As a whole, unsurprisingly, we find the same behaviour and structure, however, there are some intriguing differences. Perhaps the most interesting is the small island of instability in Figure 4.11b at around $s = 0.075$, $b = 1.1$ which was not present in the other ordering. Within this island the wave is unstable and breaks, but, curiously there is a small gap between

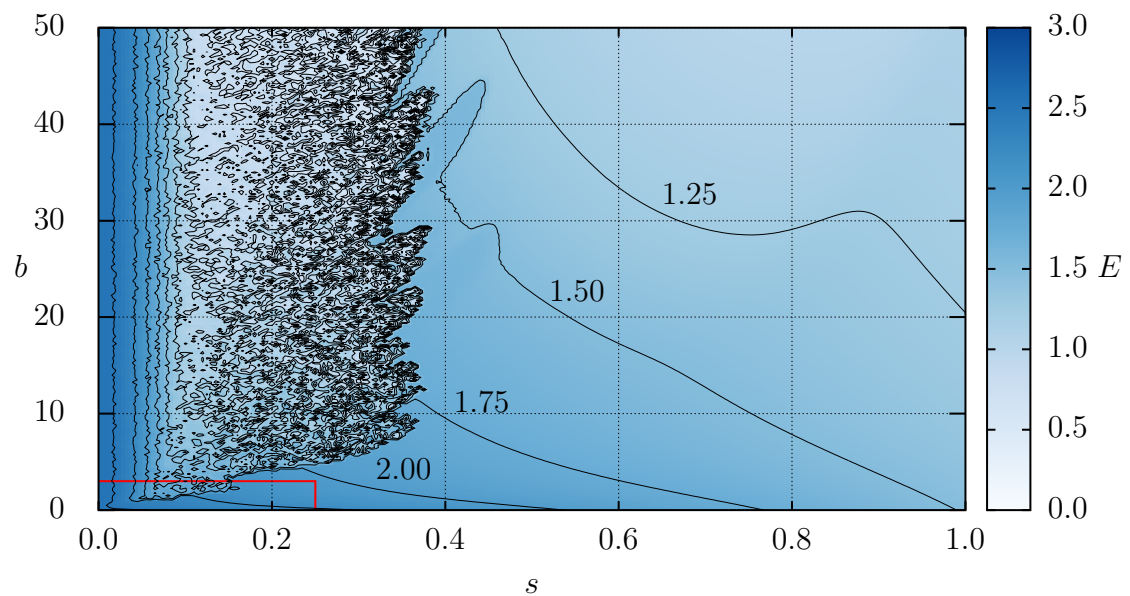
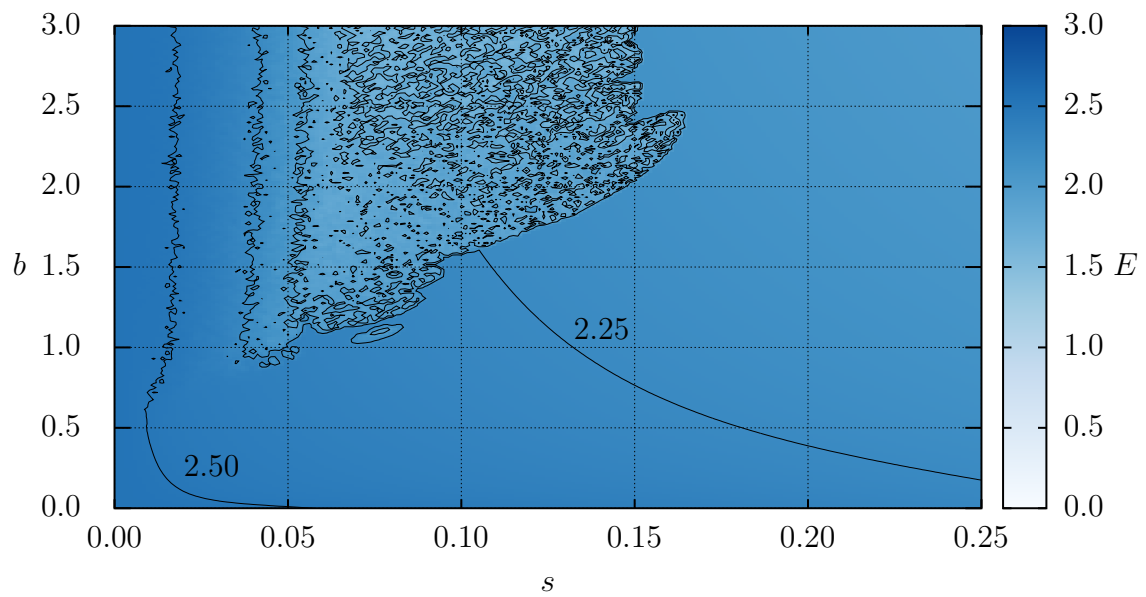
(a) Energy of the pulse within the s - b plane.(b) Regime corresponding to typical s , and b values for tuneable lasers.

Figure 4.11: Energy of the pulse after 100 cycles with the modulation and dispersion blocks switched.

this island and the main unstable region. We find more distinctions when considering the larger area in Figure 4.11a. Again, the structure and periodic nature of the boundary is similar to before, however, this boundary has shifted rightwards to a larger s value. Additionally, within the unstable region the density of the contour lines is much greater—suggesting it is in some sense more chaotic and random than with the components in their original permutation. The final main difference between the two orderings, is that in this case the energy contours are no longer monotonic functions of s . Instead we find a parabolic shape on the top contour, and two lobes on the second contour.

4.3 Chapter Summary

In this chapter we investigated how the nonlinear solution deviates from the linear solution by including the effects of the nonlinearity. We did this numerically; first we had to validate the code by comparing to the analytic result from Chapter 3. Once the code yielded the expected results for the linearized version, we incorporated the nonlinearity.

We began our investigation with the quantity of most interest—the energy. The energy of the pulse at equilibrium was shown in Figure 4.5. Generally, the results were as expected with the exception of the left-hand region. In this region, while smooth, the derivatives of the energy were very large leading to a very rough and noisy surface. It’s this region where SPM takes over and ultimately leads to the pulse becoming unstable and breaking. When considering the nonlinearity the pulse begins to interfere with itself which causes this instability.

To better understand the stability of the pulse, we turned our attention to computing the error between consecutive iterations by (4.1). This showed that the relative error within the wave breaking region is of order unity. Whereas, in the stable region the error took on values between 10^{-4} and 10^{-16} . This is because the pulse reached a steady state with a periodicity greater than 1, which was highlighted by computing the composite error, (4.2), shown in Figure 4.10.

Finally, because the components of our model do not necessarily commute with each other and the order is important, we considered the effect of swapping the dispersion and modulation components. Overall, the structure of the solutions were very similar, as we saw in Figure 4.11. There were two main differences—the first was that the boundary between stable and unstable has shifted to a larger value of the dispersion parameter, s . The second difference was that the energy, in general, was higher as in Figure 4.5.

Conclusion

By expanding upon the ideas originally proposed by Cutler [35], and Kuizenga and Siegman [36, 37, 39], we developed a nonlinear functional model for tuneable lasers. By omitting the nonlinearity, we obtain similar linearly chirped Gaussian solutions. However, a consequence of showing that Gaussians span $L^2(\mathbb{R})$ is that the linear model has been solved regardless of the choice of the modulation function.

In contrast, with the inclusion of the nonlinearity we were able to demonstrate wave breaking, and found a peculiar boundary of stability. This phenomenon has been demonstrated in a laboratory setting [15, 17, 20, 21, 46], but, previous mathematical models have been unable to capture it thus far. The nonlinearity induces SPM which injects higher frequency modes to the pulse. This causes the Fourier transform to become bimodal instead of Gaussian. As the nonlinearity increases, so too does the separation between these two modes. If this effect becomes too strong, the wave becomes incoherent and deformed, and ultimately unsustainable—the wave has broken.

The shape of this boundary between a stable pulse, and an unstable broken pulse is quite intriguing, and surprisingly sharp. At a critical s value, about 0.3 in our

simulations, the boundary becomes periodic in the parameter space—this arises from the nature of the nonlinearity. In a sense the nonlinearity is periodic in b , and thus, the stability of the solution is as well.

One of the issues experimentalists have is designing their tuneable lasers. They are uncertain how their laser will behave—and if the laser will lase at all—until they actually construct it. This model serves to provide better design principles, and how to troubleshoot should they encounter wave breaking. For example, from our results it is clear that to fix a broken wave b must be decreased, or s increased. This could be achieved by reducing the length of the optical fibre between the gain fibre and the output coupler, or by increasing $\beta_2 L_D$ by adding a second CFBG in series, respectively¹. Additionally, one could decrease the modulation time, T_M , to move through the parameter space along a ray outward from the origin. Although this would increase b , it also could increase s enough to move out of the unstable region.

5.1 Future Work

There are a few avenues to explore as a continuation of this project. The first is to compare to experimental data to validate the findings. However, due to the ultra-short duration of the pulses it becomes difficult to accurately measure the envelope and spectrum—autocorrelation methods must be used. This makes it troublesome to make the distinction between a Gaussian envelope or the generalized Gaussian envelope we've found.

An analytic development of interest is to find the asymptotic expansion for small values of the nonlinearity parameter—that is, $b \rightarrow 0$. This is likely to provide insight

¹See (3.9).

to how the nonlinearity impacts the linearized solution to better understand the manifestation of wave breaking. Furthermore, to probe the underlying structure shown in Figure 4.8 a bifurcation diagram could be constructed or analytic continuation could be used to observe the sensitivity to the parameters.

References

- [1] A. Al-Azzawi, *Fiber Optics: Principles and Advanced Practices*. CRC Press, 2 ed., 2017.
- [2] C. S. Bohun, Y. Cher, L. J. Cummings, P. Howell, T. Mitre, L. Monasse, J. Mueller, and S. Rouillon, “Modelling and Specifying Dispersive Laser Cavities,” in *Sixth Montréal Industrial Problem Solving Workshop*, pp. 11–25, 2015.
- [3] B. Burgoyne and A. Villeneuve, “Programmable Lasers: Design and Applications,” in *Proc.SPIE*, vol. 7580, 2010.
- [4] S. Yamashita, Y. Nakazaki, R. Konishi, and O. Kusakari, “Wide and Fast Wavelength-Swept Fiber Laser Based on Dispersion Tuning for Dynamic Sensing,” *Journal of Sensors*, vol. 2009, 2009.
- [5] B. Burgoyne, A. Dupuis, and A. Villeneuve, “An Experimentally Validated Discrete Model for Dispersion-Tuned Actively Mode-Locked Lasers,” *IEEE Journal of Selected Topics in Quantum Electronics*, vol. 20, pp. 390–398, Sept 2014.
- [6] W. T. Silfvast, *Laser Fundamentals*. Cambridge University Press, 2 ed., 2004.
- [7] M. F. S. Ferreira, *Nonlinear Effects in Optical Fibers*. John Wiley & Sons, Inc., 2011.
- [8] P. C. Becker, N. A. Olsson, and J. R. Simpson, *Erbium-Doped Fiber Amplifiers Fundamentals and Technology*. Academic Press, 1 ed., 1999.

- [9] A. N. Starodoumov, “Optical Fibers and Accessories,” in Malacara-Hernández and Thompson [50], pp. 633–676. Ch. 18. 2018.
- [10] G. Agrawal, *Fiber-Optic Communication Systems*. John Wiley & Sons, Inc., 3 ed., 2002.
- [11] L. Dong, M. J. Cole, A. D. Ellis, M. Durkin, M. Ibsen, V. Gusmeroli, and R. Laming, “40 Gbit/s 1.55 μm Transmission Over 109 km of Non-Dispersion Shifted Fibre with Long Continuously Chirped Fibre Gratings,” in *Conference on Optical Fiber Communications*, Optical Society of America, 1997.
- [12] H. A. Haus, *Waves and Fields in Optoelectronics*. Prentice-Hall, Inc., 1984.
- [13] M. A. Karim, “Electro-Optical and Acousto-Optical Devices,” in Malacara-Hernández and Thompson [50], pp. 409–458. Ch. 11. 2018.
- [14] D. H. Goldstein, “Anisotropic Materials,” in Malacara-Hernández and Thompson [50], pp. 695–726. Ch. 20. 2018.
- [15] G. Agrawal, *Nonlinear Fiber Optics*. Academic Press, 5 ed., 2013.
- [16] J. R. Ockendon and W. R. Hodgkins, eds., *Moving Boundary Problems in Heat Flow and Diffusion*. Oxford University Press, Mar 1975.
- [17] D. Anderson, M. Desaix, M. Lisak, and M. L. Quiroga-Teixeiro, “Wave Breaking in Nonlinear-Optical Fibers,” *J. Opt. Soc. Am. B*, vol. 9, pp. 1358–1361, Aug 1992.
- [18] B. Burgoyne, N. Godbout, and S. Lacroix, “Nonlinear Pulse Propagation in Optical Fibers Using Second Order Moments,” *Opt. Express*, vol. 15, pp. 10075–10090, Aug 2007.
- [19] E. Desurvire, *Erbium-Doped Fiber Amplifiers Principles and Applications*. John Wiley & Sons, Inc., 2002.

- [20] C. Finot, B. Kibler, L. Provost, and S. Wabnitz, “Beneficial Impact of Wave-Breaking for Coherent Continuum Formation in Normally Dispersive Nonlinear Fibers,” *J. Opt. Soc. Am. B*, vol. 25, pp. 1938–1948, Nov 2008.
- [21] J. E. Rothenberg, “Femtosecond Optical Shocks and Wave Breaking in Fiber Propagation,” *J. Opt. Soc. Am. B*, vol. 6, pp. 2392–2401, Dec 1989.
- [22] F. Kärtner, “Lecture Notes in Ultrafast Optics.” Online, Spring 2005. Massachusetts Institute of Technology: MIT OpenCourseWare.
- [23] N. M. Litchinitser, B. J. Eggleton, and D. B. Patterson, “Fiber Bragg Gratings for Dispersion Compensation in Transmission: Theoretical Model and Design Criteria for Nearly Ideal Pulse Recompression,” *Journal of Lightwave Technology*, vol. 15, pp. 1303–1313, Aug 1997.
- [24] J. Peng, H. Luo, and L. Zhan, “In-Cavity Soliton Self-Frequency Shift Ultrafast Fiber Lasers,” *Opt. Lett.*, vol. 43, pp. 5913–5916, Dec 2018.
- [25] O. V. Shtyrina, A. V. Ivanenko, I. A. Yarutkina, A. V. Kemmer, A. S. Skidin, S. M. Kobtsev, and M. P. Fedoruk, “Experimental Measurement and Analytical Estimation of the Signal Gain in an Er-Doped Fiber,” *J. Opt. Soc. Am. B*, vol. 34, pp. 227–231, Feb 2017.
- [26] I. Yarutkina, O. Shtyrina, M. Fedoruk, and S. Turitsyn, “Numerical Modeling of Fiber Lasers with Long and Ultra-long Ring Cavity,” *Opt. Express*, vol. 21, pp. 12942–12950, May 2013.
- [27] H. A. Haus, “A Theory of Forced Mode Locking,” *IEEE Journal of Quantum Electronics*, vol. 11, pp. 323–330, July 1975.
- [28] H. A. Haus, “Laser Mode Locking with Addition of Nonlinear Index,” *IEEE Journal of Quantum Electronics*, vol. 22, pp. 325–331, Feb 1986.

- [29] H. A. Haus, "Analytic Theory of Additive Pulse and Kerr Lens Mode Locking," *IEEE Journal of Quantum Electronics*, vol. 28, pp. 2086–2096, Oct 1992.
- [30] H. A. Haus, "Mode-Locking of Lasers," *IEEE Journal of Selected Topics in Quantum Electronics*, vol. 6, pp. 1173–1185, Nov 2000.
- [31] K. Tamura and M. Nakazawa, "Dispersion-Tuned Harmonically Mode-Locked Fiber Ring Laser for Self-Synchronization to an External Clock," *Opt. Lett.*, vol. 21, pp. 1984–1986, Dec 1996.
- [32] N. G. Usechak and G. P. Agrawal, "Rate-Equation Approach for Frequency-Modulation Mode Locking using the Moment Method," *J. Opt. Soc. Am. B*, vol. 22, pp. 2570–2580, Dec 2005.
- [33] H. A. Haus, "Theory of Soliton Stability in Asynchronous Modelocking," *Journal of Lightwave Technology*, vol. 14, pp. 622–627, April 1996.
- [34] H. A. Haus, J. G. Fujimoto, and E. P. Ippen, "Structures for Additive Pulse Mode Locking," *J. Opt. Soc. Am. B*, vol. 8, pp. 2068–2076, Oct 1991.
- [35] C. C. Cutler, "The Regenerative Pulse Generator," in *Proceedings of the IRE*, IEEE, Feb 1955.
- [36] D. J. Kuizenga and A. E. Siegman, "FM and AM Mode Locking of the Homogeneous Laser - Part I: Theory," *IEEE Journal of Quantum Electronics*, vol. 6, pp. 694–708, Nov 1970.
- [37] A. E. Siegman and D. J. Kuizenga, "Simple Analytic Expressions for AM and FM Modelocked Pulses in Homogenous Lasers," *Appl. Phys. Lett.*, pp. 181–182, Mar 1969.
- [38] D. J. Kuizenga and A. E. Siegman, "FM and AM Mode Locking of the Homogeneous Laser - Part II: Experimental Results in a Nd:YAG Laser with Internal

- FM Modulation,” *IEEE Journal of Quantum Electronics*, vol. 6, pp. 709–715, Nov 1970.
- [39] D. J. Kuizenga and A. E. Siegman, “FM-Laser Operation of the Nd:YAG Laser,” *IEEE Journal of Quantum Electronics*, vol. 6, pp. 673–677, Nov 1970.
- [40] O. E. Martinez, R. L. Fork, and J. P. Gordon, “Theory of Passively Mode-Locked Lasers Including Self-Phase Modulation and Group-Velocity Dispersion,” *Opt. Lett.*, vol. 9, pp. 156–158, May 1984.
- [41] O. E. Martinez, R. L. Fork, and J. P. Gordon, “Theory of Passively Mode-Locked Lasers for the Case of a Nonlinear Complex-Propagation Coefficient,” *J. Opt. Soc. Am. B*, vol. 2, pp. 753–760, May 1985.
- [42] A. M. Dunlop, W. J. Firth, and E. M. Wright, “Pulse Shapes and Stability in Kerr and Active Mode-Locking (KAML),” *Opt. Express*, vol. 2, pp. 204–211, Mar 1998.
- [43] L. Debnath and D. Bhatta, *Integral Transforms and Their Applications*. Chapman & Hall/CRC Press, 2 ed., 2007.
- [44] I. S. Gradshteyn and I. M. Ryzhik, *Table of Integrals, Series, and Products*. Academic Press, 7 ed., 2007.
- [45] B. Burgoyne. Private Communication, 2018.
- [46] W. J. Tomlinson, R. H. Stolen, and A. M. Johnson, “Optical Wave Breaking of Pulses in Nonlinear Optical Fibers,” *Opt. Lett.*, vol. 10, pp. 457–459, Sept 1985.
- [47] S. Li and K. T. Chan, “Electrical Wavelength Tunable and Multiwavelength Actively Mode-Locked Fiber Ring Laser,” *Applied Physics Letters*, vol. 72, no. 16, pp. 1954–1956, 1998.

- [48] K. Tamura, E. P. Ippen, H. A. Haus, and L. E. Nelson, “77-fs Pulse Generation from a Stretched-Pulse Mode-Locked All-Fiber Ring Laser,” *Opt. Lett.*, vol. 18, pp. 1080–1082, Jul 1993.
- [49] Q. Chen, N. Lu, and F. Jiang, “Characterization of the Dispersion of Chirped Fiber Bragg Grating Through Fourier Transform Spectrometry Method,” in *Proc. SPIE*, vol. 6837, 2008.
- [50] D. Malacara-Hernández and B. J. Thompson, eds., *Advanced Optical Instruments and Techniques*, vol. 2 of *Handbook of Optical Engineering*. CRC Press, 2 ed., 2018.
- [51] M. Abramowitz and I. A. Stegun, eds., *Handbook of Mathematical Functions*. United States Government Publishing Office, 10 ed., 1972.
- [52] T. Gowers, ed., *The Princeton Companion to Mathematics*. Princeton University Press, 2008.
- [53] R. M. Corless, G. H. Gonnet, D. E. G. Hare, D. J. Jeffrey, and D. E. Knuth, “On the Lambert W function,” *Advances in Computational Mathematics*, vol. 5, Dec 1996.
- [54] J. B. Conway, *A Course in Functional Analysis*, vol. 96 of *Graduate Texts in Mathematics*. Springer-Verlag New York Inc., 1 ed., 1985.
- [55] R. Courant and D. Hilbert, *Methoden der Mathematischen Physik*, vol. I. Julius Springer, 1924.
- [56] J. Teuwen, “A Cornucopia of Hermite Polynomials,” *Research Gate*, March 2016.
- [57] U. W. Hochstrasser, “Orthogonal Polynomials,” in Abramowitz and Stegun [51], pp. 771–802. Ch. 22. 1972.

- [58] E. Kreyszig, *Introductory Functional Analysis with Applications*. John Wiley & Sons, Inc., 1978.
- [59] G. Szegö, *Orthogonal Polynomials*, vol. XXIII of *American Mathematical Society Colloquium Publications*. American Mathematical Society, 4 ed., 1975.
- [60] D. H. Griffel, *Applied Functional Analysis*. Dover Publications, Inc., 2 ed., 2002.
- [61] A. N. Kolmogorov and S. V. Fomin, *Elements of the Theory of Functions and Functional Analysis*, vol. 2. Graylock Press, 1 ed., 1960.
- [62] J. C. P. Miller, “Parabolic Cylinder Functions,” in Abramowitz and Stegun [51], pp. 685–720. Ch. 19. 1972.
- [63] N. Higson and J. Roe, “Operator Algebras,” in Gowers [52], pp. 510–523. Ch. IV.15. 2008.
- [64] C. Calcaterra, “Linear Combinations of Gaussians with a Single Variance are Dense in L^2 ,” in *Proceedings of the World Congress on Engineering*, vol. II, 2008.
- [65] C. Calcaterra and A. Boldt, “Approximating with Gaussians,” *ArXiv*, May 2008. [arXiv:0805.3795](https://arxiv.org/abs/0805.3795).
- [66] D. Zwillinger, *Handbook of Differential Equations*. Academic Press, 2 ed., 1992.

Appendix A

The Lambert W Function

The Lambert W function is defined to be the inverse of the function $f(x) = xe^x$; its graph is shown in Figure A.1. In other words, if $z = xe^x$ then $x = W(z)$. Notice that by combining these relations we obtain the identities

$$z = W(z)e^{W(z)}, \quad x = W(xe^x). \quad (\text{A.1})$$

This function is called the Lambert W function because it is the logarithm of a special instance of Lambert's series—the letter W is used because of the work done by E. M. Wright [53].

Notice that the original function, $f(x) = xe^x$, is *not* injective, and as a consequence, the W function is multi-valued on the interval $[-1/e, 0]$. To alleviate this, occasionally the branch $W(x) \geq -1$ is denoted W_0 and is called the principal or upper branch, whereas the branch $W(x) < -1$ is denoted W_{-1} and is called the lower branch. However, in this work the W function will only take positive real values and so this distinction is not needed.

The Lambert W function has applications in various areas of math and physics [53]

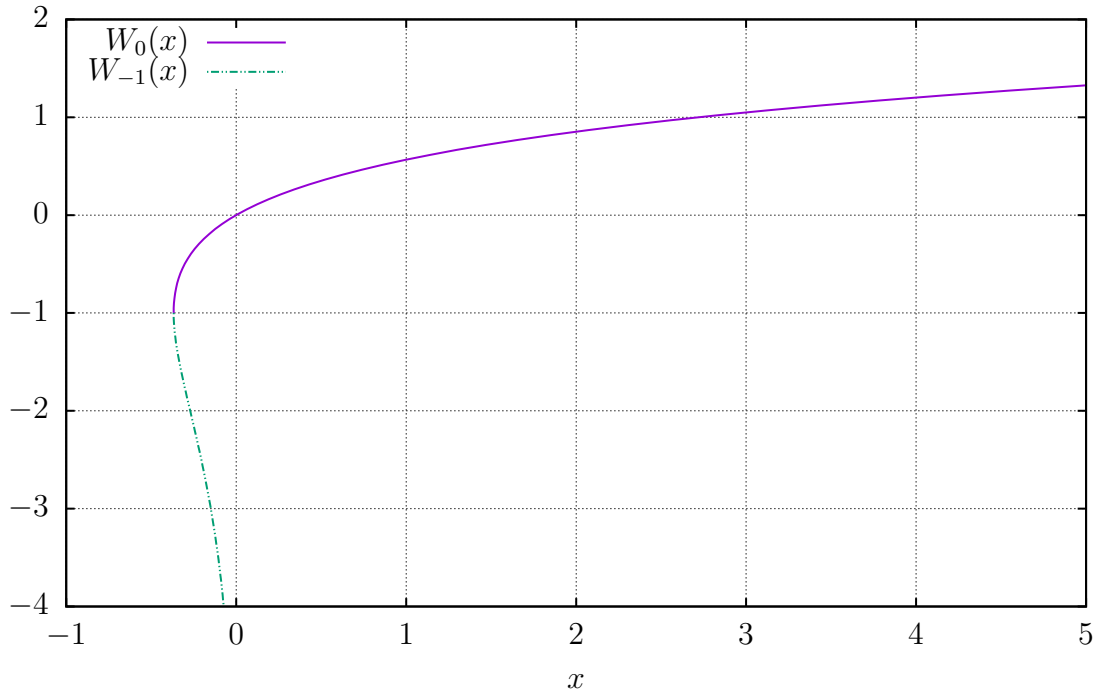


Figure A.1: The two branches of the Lambert W function.

including:

- Jet fuel problems
- Combustion problems
- Enzyme kinetics problems
- Linear constant coefficient differential delay equations
- Volterra equations.

Primarily, the W function arises when solving iterated exponentiation or certain algebraic equations. For example, consider the equation $z = x^x$. By taking the logarithm of each side we have

$$\log z = x \log x,$$

$$= \log x e^{\log x},$$

which after applying the W function reduces to $W(\log z) = \log x$ by (A.1). Finally, x as a function of z can be written as $x = \exp(W(\log z))$.

B

Appendix

Span of Gaussians in $L^2(\mathbb{R})$

In order to show that Gaussians span $L^2(\mathbb{R})$, we shall start our analysis with the span of the Hermite polynomials in $L^2(\mathbb{R})$. Typically the Hermite polynomials are recursively defined as [54–56]

$$H_n(x) := (-1)^n e^{x^2} \frac{d^n}{dx^n} e^{-x^2},$$

with the inner product¹

$$\langle f, g \rangle = \int_{\mathbb{R}} f(x)g(x)e^{-x^2} dx,$$

where e^{-x^2} is the weighting function. This is so that

$$\langle H_m, H_n \rangle = \sqrt{\pi} 2^n n! \delta_{m,n},$$

where $\delta_{m,n}$ is the Kronecker δ function. Therefore, the Hermite polynomials form an orthogonal set [55–59]. Consider instead, the Gaussian–Hermite polynomials from

¹The complex conjugate of g is omitted since the functions dealt with are real.

(2.10):

$$\tilde{H}_n(x) := e^{-x^2/2} H_n(x),$$

with the inner product

$$\langle f, g \rangle = \int_{\mathbb{R}} f(x)g(x) dx,$$

notice that the weighting function has been absorbed into the Hermite polynomials.

We shall now show that the set of Gaussian–Hermite polynomials spans $L^2(\mathbb{R})$.

Theorem B.1. *The set of Gaussian–Hermite polynomials, $\mathcal{G}(\mathbb{R}) = \{\tilde{H}_n(x) : x \in \mathbb{R}, n \in \mathbb{N}\}$, spans $L^2(\mathbb{R})$.*

Proof. The Gaussian–Hermite polynomials are an orthogonalization of the set $\Xi = \{x^n e^{-x^2/2} : x \in \mathbb{R}, n \in \mathbb{N}\}$, and therefore, have the same span [58, 59]. Thus, it is sufficient to show that Ξ spans $L^2(\mathbb{R})$. Suppose there exists an $f \in L^2(\mathbb{R})$ such that $\langle f, \tilde{H}_n \rangle = 0$ for all n , or equivalently, that $\langle f, g_n \rangle = 0$ for $g_n(x) = x^n e^{-x^2/2}$ for all n so that it is not in the span of $\mathcal{G}(\mathbb{R})$.

Let us now consider the function [55, 56, 59]

$$F(z) = \frac{1}{\sqrt{2\pi}} \int_{\mathbb{R}} f(x) e^{zx} e^{-x^2/2} dx,$$

noting that $f(x) e^{zx} e^{-x^2/2} \in L^2(\mathbb{R})$ by the Cauchy–Schwarz inequality [60, 61], so F converges, and that F is holomorphic. The first exponential can be expanded into its

Maclaurin series, then with Fubini's theorem we obtain

$$F(z) = \frac{1}{\sqrt{2\pi}} \sum_{n=0}^{\infty} \frac{z^n}{n!} \int_{\mathbb{R}} f(x) x^n e^{-x^2/2} dx.$$

Recall, that by assumption

$$\int_{\mathbb{R}} f(x) x^n e^{-x^2/2} dx = \langle f, g_n \rangle = 0,$$

for all n and so $F(z) \equiv 0$. We now notice that

$$0 = F(z) = F(i\omega) = \mathcal{F}\left\{f e^{-x^2/2}\right\},$$

and now it is clear that $f(x)e^{-x^2/2} = 0$ almost everywhere, therefore, $f(x) = 0$ almost everywhere. \square

Alternatively, without much difficulty it can be shown that the Gaussian–Hermite polynomials satisfy

$$\frac{d^2 \tilde{H}_n(x)}{dx^2} - (x^2 - 2n - 1) \tilde{H}_n(x) = 0. \quad (\text{B.1})$$

This has the form of the parabolic cylinder functions [62], and indeed the Gaussian–Hermite polynomials can be expressed in terms of parabolic cylinder functions [57, 62]. Moreover, (B.1) can also be written in Sturm–Liouville form as

$$\frac{d}{dx} \left(p(x) \cdot \frac{d\tilde{H}_n(x)}{dx} \right) + (1 - x^2) \tilde{H}_n(x) = -2n \tilde{H}_n(x), \quad p(x) = 1.$$

By the spectral theorem [58, 60, 63], this suggests that the Gaussian–Hermite polynomials form an orthogonal set with the weighting function $w(x) = 1$, and are complete in $L^2(\mathbb{R})$. Using this result, we can now show that Gaussian functions also span $L^2(\mathbb{R})$

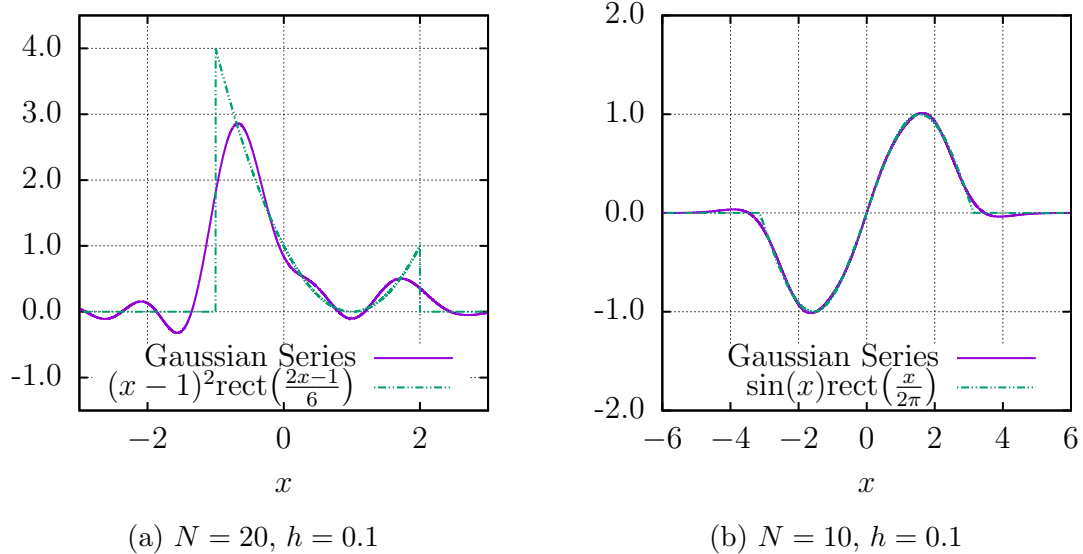


Figure B.1: Two examples of Gaussian series.

with the following theorem.

Theorem B.2. *Gaussians of a single variance span $L^2(\mathbb{R})$.*

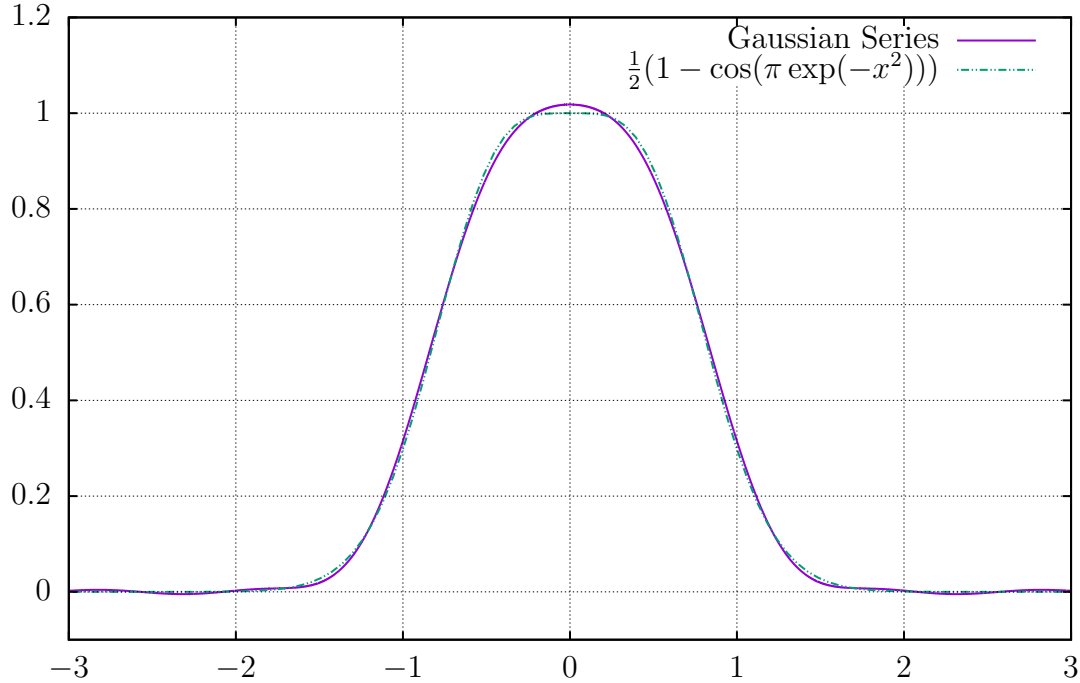
Proof. Theorem B.1 showed that any square integrable function can be expressed as

$$f(x) = \sum_{n=0}^{\infty} a_n \tilde{H}_n(x).$$

Recall that $\tilde{H}_n(x)$ has a polynomial as well as a Gaussian component. Without loss of generality we assumed the Gaussian has variance $\frac{1}{2}$ for convenience. We can effectively remove the polynomial dependence by using a similar idea to [64, 65]. We shall expand the Gaussian–Hermite polynomials using their definition

$$f(x) = \sum_{n=0}^{\infty} a_n (-1)^n e^{x^2/2} \frac{d^n}{dx^n} e^{-x^2}.$$

Finally, we can rewrite the derivatives using central differences [66] so that our func-

Figure B.2: Gaussian series with $N = 20$, $h = 0.1$.

tion can be expressed as

$$f(x) = \sum_{n=0}^{\infty} a_n (-1)^n e^{x^2/2} \left[\lim_{h \rightarrow 0} \frac{1}{h^n} \sum_{i=0}^n (-1)^i \binom{n}{i} \exp\left(-\left(x + h\left(\frac{n}{2} - i\right)\right)^2\right) \right]. \quad (\text{B.2})$$

□

Two examples of Gaussian series from (B.2) are shown in Figure B.1. These examples are taken from [64, 65], however, we achieve similar or better approximations with either fewer terms, or with an h value an order of magnitude larger. There are two reasons for this, first, we use central difference as opposed to backwards difference yielding a convergence of $\mathcal{O}(h^2)$ instead of $\mathcal{O}(h)$. Furthermore, because [64, 65] used backwards differences, the means of the Gaussians are all non-negative, whereas with central differences, our Gaussians' means are both positive and negative—this leads to smaller coefficients, and better numerical stability. Moreover, Figure B.2 shows

the Gaussian series for the modulation function

$$M(T) = \frac{1}{2} \left(1 - \cos(\pi e^{-x^2}) \right),$$

used in [2, 45].

C

Appendix

Code

```
1 #####  
2 #      Brady Metherall  
3 #      MSc Thesis  
4 #####  
5 ...  
6 This is the code used for my MSc thesis. This code  
7 is separated into four parts each described below.  
8 ...  
9  
10 #####  
11 #  Part I  
12 #####  
13 ...  
14 Function definitions and initialization  
15 ...  
16  
17 import numpy as np
```

```
18 import scipy.special.lambertw as W
19 import matplotlib.pyplot as plt
20 import time
21 from scipy.optimize import curve_fit
22
23 def func(x, a, b):
24     return a * np.exp(-x**2 / (2 * b**2))
25
26 def Energy(A, dx):
27     return np.trapz(np.real(A * np.conj(A)), dx = dx)
28
29 # Functions for each component
30 def Gain(A, E, a = 8000):
31     return np.real(np.sqrt(W(a * E * np.exp(E)) / E)) * A
32
33 def Loss(A, h = 0.04):
34     return h * A
35
36 def Mod(A, T):
37     return np.exp(-T**2 / 2) * A
38
39 def Fibre(A, b = 1.0):
40     return np.exp(1j * b * np.abs(A)**2) * A
41
42 def Disp(A, T, s = 0.1):
43     F = np.fft.fft(A)
44     F = F * (np.abs(F) > 10**-4) # Numerical stability
```

```

45      dw = np.pi / T[-1]
46      w = np.fft.fftfreq(len(A)) * len(A) * dw
47      return np.fft.ifft(F * np.exp(1j * w**2 * s**2))
48
49 # 1 round trip
50 def Loop(A, T, dx, s, b, switch = False):
51     A = Loss(A)
52     if not switch:
53         A = Disp(A, T, s)
54         A = Mod(A, T)
55     else:
56         A = Mod(A, T)
57         A = Disp(A, T, s)
58     A = Gain(A, Energy(A, dx))
59     A = Fibre(A, b)
60     return A
61
62 N = 25 # Number of loops of the circuit
63 p = 2**12 # Number of points in the discretization
64 width = 64 # Size of window
65 E0 = 0.1 # Initial energy
66
67 # Initialization
68 T = np.linspace(-width, width, p, endpoint = False)
69 dx = T[1] - T[0]
70 A0 = 1 / np.cosh(2 * T) * np.exp(1j * np.pi / 4)
71 A0 = np.sqrt(E0 / Energy(A0, dx)) * A0 # Normalize

```

```
72 E = np.zeros(N)
73 data = np.zeros((2 * N, p))
74 A = A0
75
76 part = 6 # Select which part of the code to run
77
78 if part == 2:
79     #####
80     # Part II
81     #####
82     ...
83     On the fly animation of single realizations
84     ...
85     plt.ion()
86     fig = plt.figure()
87     ax = fig.add_subplot(111)
88     line1, = ax.plot(T, np.real(A), 'r-', label = 'Real')
89     line2, = ax.plot(T, np.imag(A), 'b-', label = 'Imaginary',
90
91     dw = np.pi / T[-1]
92     line3, = ax.plot(T, np.abs(A), 'g-', label = 'Magnitude')
93
94     fig.canvas.draw()
95     fig.canvas.flush_events()
96
97     plt.legend()
```

```
98     plt.xlim(-2, 2)
99     plt.ylim(-4, 4)
100
101    # N round trips of the laser
102    for i in range(N):
103        # Animate the plot
104        line1.set_ydata(np.real(A))
105        line2.set_ydata(np.imag(A))
106        line3.set_ydata(np.abs(A))
107        fig.canvas.draw()
108        fig.canvas.flush_events()
109        #time.sleep(2)
110        print i
111
112        A = Loop(A, T, dx, 0.15, 0.5)
113        E[i] = Energy(A, dx)
114        #time.sleep(0.5)
115
116        #np.savetxt('E.dat', E)
117
118        dw = np.pi / T[-1]
119        w = np.fft.freq(len(A)) * len(A) * dw
120
121        print np.trapz(T**2 * abs(A), dx=dx) / np.trapz(abs(A),
122                                                       dx=dx)
123        #np.savetxt('Linear_Solution.dat', np.vstack((T, np.real(
```

```
A) , np.imag(A) , np.abs(A) , w, np.abs(np.fft.fft(A)) , np.
angle(A))).T)

124

125 elif part == 3:
126     #####
127     # Part III
128     #####
129     ''
130     Run the simulation for an nxn grid in s-b space
131     ''
132     n = 501
133     #z = np.zeros((n**2, 4))
134     zoom = True
135     step = 1
136
137     if zoom:
138         s = np.linspace(0, 0.25, num = n)
139         #b = np.logspace(3.0, 5.0, num = n)
140         b = np.linspace(0, 3, num = n)
141     else:
142         s = np.linspace(0, 1, num = n)
143         #b = np.logspace(3.0, 6.0, num = n)
144         b = np.linspace(0, 50, num = n)
145
146     #filename = 'Step' + str(step) + '.dat'
147     filename = 'Step_Big.dat'
148     #filename = 'Moments.dat'
```

```

149     open( filename , 'w' ) . close ( )
150     f = open( filename , 'ab' )
151
152     for k in range(n):
153         print k
154         z = np.zeros((n, 5))
155         for j in range(n):
156             A0 = 1 / np.cosh(2 * T) * np.exp(1j * np.pi / 4)
157             A0 = np.sqrt(E0 / Energy(A0, dx)) * A0 #
                                         Normalize
158             A = A0
159 #             flag = [0, 0, 0]
160 #             itera = np.array([100, 100, 100])
161 #             for i in range(100 / step + 1):
162 #                 old = np.abs(A)
163 #                 for lnum in range(step):
164 #                     A = Loop(A, T, dx, s[j], b[k], switch =
                                         False)
165 #                     new = np.abs(A)
166 #                     if (flag[0] == 0) and (np.sqrt(np.trapz((old
                                         - new)**2, dx = dx)) < 10**-3): # L2
167 #                         itera[0] = i
168 #                         flag[0] = 1
169 #                     elif (flag[1] == 0) and (np.trapz(np.abs(old
                                         - new), dx = dx) < 10**-3): # L1
170 #                         itera[1] = i
171 #                         flag[1] = 1

```

```
172 #           elif (flag[2] == 0) and (np.max(np.abs(old -  
new)) < 10**-3): # Infinity  
173 #               itera[2] = i  
174 #               flag[2] = 1  
175 #       z[j] = s[j], b[k], itera[0], itera[1], itera[2],  
#       np.sqrt(np.trapz((old - new)**2, dx = dx)) / np.sqrt(np.  
#       trapz(old**2, dx = dx)), Energy(A, dx)  
176  
177     for i in range(500):  
178         A = Loop(A, T, dx, s[j], b[k], switch = False  
    )  
179         old = np.abs(A)  
180         A = Loop(A, T, dx, s[j], b[k], switch = False)  
181         new = np.abs(A)  
182  
183         err = np.sqrt(np.trapz((new - old)**2, dx = dx) /  
#         np.trapz(new**2, dx = dx))  
184         sigma = np.trapz(T**2 * abs(A), dx = dx) / np.  
#         trapz(abs(A), dx = dx)  
185         kurt = np.trapz(T**4 * abs(A), dx = dx) / np.  
#         trapz(T**2 * abs(A), dx = dx)  
186  
187         z[j] = s[j], b[k], sigma, kurt / sigma, err  
188  
189         np.savetxt(f, z)  
190         f.write('\n')  
191
```

```
192     f.close()
193
194 elif part == 4:
195     #####
196     # Part IV
197     #####
198     ,
199     Compute features of linear model (E, P, sigma, C, phi)
200     ,
201     n = 50
202     z = np.zeros((n, 6))
203     s = np.linspace(0, 3, num = n)
204
205     for j in range(n):
206         A0 = 1 / np.cosh(2 * T) * np.exp(1j * np.pi / 4)
207         A0 = np.sqrt(E0 / Energy(A0, dx)) * A0 # Normalize
208         A = A0
209         for i in range(25):
210             old = np.angle(A[len(A)/2])
211             A = Loop(A, T, dx, s[j], 0, switch = False)
212             new = np.angle(A[len(A)/2])
213             while old > new:
214                 old -= 2 * np.pi
215             r, sigma = curve_fit(func, T, np.abs(A))[0]
216             z[j] = s[j], Energy(A, dx), np.abs(A)[len(A)/2]**2,
sigma, -np.gradient(np.gradient(np.angle(A), dx), dx)[len(A)/2] * sigma**2, new - old
```

```
217
218     np.savetxt( 'Linear.dat' , z)
219
220 elif part == 5:
221     ######
222     # Part V
223     #####
224     ,
225     Compute variance for various b values
226     ,
227     n = 100
228     s = np.linspace(0, 2, num = n)
229     b = [0.0, 0.1, 0.5, 1.0, 2.0, 5.0, 10.0]
230     m = len(b)
231     z = np.zeros((n, m + 1))
232     z2 = np.zeros((n, m + 1))
233     sigma = np.zeros(m)
234     kurt = np.zeros(m)
235
236     for j in range(n):
237         A0 = 1 / np.cosh(2 * T) * np.exp(1j * np.pi / 4)
238         A0 = np.sqrt(E0 / Energy(A0, dx)) * A0 # Normalize
239         A = A0
240         for k in range(m):
241             for i in range(50):
242                 A = Loop(A, T, dx, s[j], b[k], switch = False
243             )
```

```
243         old = np.abs(A)
244         A = Loop(A, T, dx, s[j], b[k], switch = False)
245         new = np.abs(A)
246         err = np.sqrt(np trapz((old - new)**2, dx = dx) /
247                         np trapz(new**2, dx = dx))
247         if b[k] == 0 and s[j] < 0.06:
248             sigma[k] = 2 * s[j] * (1.0 - s[j])
249             kurt[k] = np.nan
250         elif err > 0.005:
251             sigma[k] = np.nan
252             kurt[k] = np.nan
253         else:
254             sigma[k] = np trapz(T**2 * abs(A), dx = dx) /
254                 np trapz(abs(A), dx = dx)
255             kurt[k] = np trapz(T**4 * abs(A), dx = dx) /
255                 np trapz(T**2 * abs(A), dx = dx)
256             z[j] = np.hstack((s[j], sigma))
257             z2[j] = np.hstack((s[j], kurt / sigma))
258
259             np.savetxt('NL_Var.dat', z)
260             np.savetxt('NL_Kurt.dat', z2)
261
262 elif part == 6:
263     #####
264     # Part VI
265     #####
266     ''',
```

```
267     Compute convergence
268     ...
269     n = 3
270     num_iter = 100
271     s = np.linspace(0, 0.225, num = n+1)+0.025
272     #b = 5*s
273     err = np.zeros((n+1, num_iter))
274
275     print s
276     #print b
277
278     for j in range(n+1):
279         A0 = 1 / np.cosh(2 * T) * np.exp(1j * np.pi / 4)
280         A0 = np.sqrt(E0 / Energy(A0, dx)) * A0 # Normalize
281         A = A0
282         for i in range(num_iter):
283             old = np.abs(A)
284             A = Loop(A, T, dx, s[j], 0.5, switch = False)
285             new = np.abs(A)
286             err[j, i] = np.sqrt(np.trapz((old - new)**2, dx =
287                                         dx) / np.trapz(new**2, dx = dx))
288     np.savetxt('ROC.dat', err.T)
289
290 else:
291     print 'Please enter a valid part number (2--6)',
```